Near-zero modes in condensate phases of the Dirac theory on the honeycomb lattice

Doron L. Bergman and Karyn Le Hur
Department of Physics, Yale University, New Haven, Connecticut 06520-8120, USA
(Received 18 June 2008; revised manuscript received 7 April 2009; published 22 May 2009)

We investigate a number of fermionic condensate phases on the honeycomb lattice to determine whether topological defects (vortices and edges) in these phases can support bound states with zero energy. We argue that topological zero modes bound to vortices and at edges are not only connected, but should in fact be *identified*. Recently, it has been shown that the simplest *s*-wave superconducting state for the Dirac fermion approximation of the honeycomb lattice at precisely half filling, supports zero modes inside the cores of vortices [P. Ghaemi and F. Wilczek, arXiv:0709.2626 (unpublished)]. We find that within the continuum Dirac theory the zero modes are not unique, either to this phase or to half filling. In addition, we find the *exact* wave functions for vortex bound zero modes, as well as the complete edge state spectrum of the phases we discuss. The zero modes in all the phases we examine have even-numbered degeneracy, and as such pairs of any Majorana modes are simply equivalent to one ordinary fermion. As a result, contrary to bound-state zero modes in p_x+ip_y superconductors, vortices here do *not* exhibit non-Abelian exchange statistics. The zero modes in the pure Dirac theory are seemingly topologically protected by the effective low-energy symmetry of the theory, yet on the original honeycomb lattice model these zero modes are split, by explicit breaking of the effective low-energy symmetry.

DOI: 10.1103/PhysRevB.79.184520 PACS number(s): 74.20.Rp, 05.30.Pr, 03.67.Lx

I. INTRODUCTION

In recent years, p_x+ip_y fermionic condensate states have received much attention due to the expectation that vortices in this state will exhibit non-Abelian (Braiding) statistics[1–6] and their potential applicability to topological quantum computing.[7,8] A frantic experimental effort to observe these effects is currently under way.[9,10] The non-Abelian effects are caused by the presence of quasiparticle zero modes (states with energy precisely at the Fermi level) bound to vortex cores.[1–5,11–14] These zero modes appear at sample edges as well,[1,15,16] and we will refer to them collectively as topological zero modes.

Zero modes in any BCS (Bardeen-Cooper-Schrieffer) mean-field Hamiltonian[1–3] can always be expressed as Majorana fermions. Pairs of Majorana states will combine to form single fermionic degrees of freedom, which can then be occupied or not. The p_x+ip_y superconducting (SC) states allow *single* zero modes bound to vortices (of unit vorticity). Therefore, fermionic states can only be formed by a superposition of two zero modes, bound to *different* vortices. In this way, these fermionic modes provide a natural entangled state between two spatially separated objects (the vortices).[2] This entanglement is the source of the non-Abelian mutual statistics, when moving one vortex adiabatically around another.

The apparent rarity of p_x+ip_y superconducting states has made difficult the effort to observe these zero modes in experiment. It would, therefore, prove useful to have further candidate states for displaying non-Abelian statistics, which could then be searched for experimentally.

The topological zero modes in the p_x+ip_y state are found as solutions of a set of coupled Dirac-type Bogoliubov-de-Gennes (BdG) equations. The source of the Dirac-type behavior is the symmetry of the p_x+ip_y superconducting order parameter. An alternative way to end up with BdG equations of the form of a Dirac equation, one which does *not* require the pairing function to be of the p_x+ip_y form, is to have a kinetic-energy term that is of the Dirac form. The most celebrated example where this occurs is in the honeycomb lattice tight-binding model, where close to half filling the band structure has Dirac-type dispersion, and the behavior of the system can be approximated by two flavors of Dirac fermions. The effective Dirac-type dispersion has been experimentally observed in monolayer graphene.[17] With the Dirac-type behavior of the BdG equations already guaranteed in this approximation, we are now free to ask whether zero modes exist in vortex cores of a whole variety of superconducting states on the honeycomb lattice. The simplest state one could consider is the *s*-wave spin-singlet-pairing state. Some time ago,[18] it was shown that this same superconducting state in a (square) lattice model with Dirac dispersion near the Fermi energy supported zero modes bound to vortex cores. More recently[19] zero modes were shown to exist (bound to vortex cores) in this state, in the Dirac continuum theory of the honeycomb lattice at precisely half filling. These findings are in stark contrast to the behavior of two-dimensional (2D) *s*-wave superconductor vortices in fermionic systems with simple quadratic dispersion, where no zero modes exist.[4,20]

Following this radically different result, in this article, we will investigate other geometries and phases for possible presence of topological zero modes. In addition, we will determine whether the zero modes appear in the actual lattice model.

Even the simplest effective attraction between fermions can cause a superconducting state to appear. However, the precise nature of the phase, namely, the symmetry of the order parameter, depends on the details of the effective interaction. In Ref. 21 it was shown in a simple mean-field analysis that fermions on the honeycomb lattice paired in spin singlets may support not only an *s*-wave state, but also an effective p_x+ip_y state, as well as a mixed *s*-wave/p_x+ip_y phase (and earlier work[22] also suggested a *p*-wave supercon-

ducting state may appear in graphene). Given the evidence of zero modes in the s-wave phase at half filling,[19] it is interesting to explore whether the p_x+ip_y spin-singlet phase may also support zero modes, as well as whether these zero modes are peculiar to the half-filling point (recently[23] it was shown that s-wave superconductivity is far more likely to appear in a fermionic system in the honeycomb lattice away from half filling). We will show in this manuscript that zero modes appear in the Dirac continuum theory in both the s-wave and the p_x+ip_y phase, even when deviating from the special half filling point (the p_x+ip_y state is in fact gapped only when the fermions are *away* from half filling). We also demonstrate that the zero modes we find are fourfold degenerate, and so fermionic modes can be formed by pairs on the *same* vortex. The mechanism for entanglement between vortices is, therefore, unfortunately lost, and no non-Abelian effects are expected in these systems. Note that it is not obvious that no condensate phase of fermions on the honeycomb lattice will exhibit non-Abelian statistics.

As mentioned above, in the p_x+ip_y state (with the regular quadratic kinetic energy) it is known that the zero modes bound to vortex cores appear in conjunction with edge states zero modes. We argue in this manuscript that this connection is in fact quite general, and that vortex-core topological zero modes and edge state zero modes should in fact be *identified*. We demonstrate this in the superconducting states we analyze here, by finding the low-energy edge states of each phase. As expected, we find precise correspondence with the vortex-core bound states—in both spin-singlet phases, there exist four zero modes. A further signature of the identification of the vortex and edge states is that the wave functions have all the same physical parameters—the same exponential decay lengths, as well the same oscillation length scales (when those exist).

A perhaps simpler indication of whether zero modes can appear at the edges or vortex cores of a given SC state, is to consider the superconducting-normal-superconducting (SNS) junction,[24] with some phase difference ϕ between the SC droplets. We find that as in the regular p_x+ip_y state,[24] zero modes appear only when $\phi=\pi$. As we will see, the edge-state calculation we employ in the continuum limit is limited in the type of honeycomb lattice edge it can be used for. For this reason the SNS junction calculation is useful—it shows that at least within the continuum limit the precise alignment of the edge is immaterial. We will find that the number of zero modes found in the SNS geometry is eight rather than four, giving us the first hint that details of boundary conditions are important in this problem—the SNS junction geometry has extra symmetries, compared with the edge and vortex cases.

The zero modes we will uncover in what follows, all have an even degeneracy. In general (for unit vorticity), only single SC quasiparticle zero modes are topologically protected to all possible perturbations; however, if there is a symmetry mandated degeneracy, which is not broken by any of the perturbations, a degenerate set of zero modes can still be protected to perturbations, and hence topologically protected (modulo symmetry mandated degeneracy). We begin the main body of our manuscript with a discussion of this distinction in general settings.

In our case, the fourfold degeneracy is mandated by the symmetries of the Dirac continuum theory. However, the full symmetry is *not* present in the underlying lattice model, and so there is a danger that the zero modes can appear in the continuum model, but *not* in the lattice model. By numerical diagonalization of the lattice model, we find indeed this is the case—the zero modes do not exist in the lattice model.

The remainder of our manuscript is organized as follows. In Sec. II we discuss topological protection of zero modes in conjunction with symmetry mandated degeneracy. In Sec. III we present our general argument for identifying zero modes bound to vortex cores and at sample edges. We then proceed to Sec. IV, where we present the honeycomb lattice BCS model, describe a number of possible superconducting states, and then set up a continuum limit for the model, which allows us to perform explicit calculations looking for zero modes in the SNS junction (Sec. V), the edge states (Sec. VI), and finally in the vortex cores (Sec. VII). We present the results of a numerical calculation on the precise honeycomb lattice BCS model in Sec. VIII. In Sec. IX we proceed to discuss a possible experimental realization of superconducting states on the honeycomb lattice. We then discuss Zeeman splitting in Sec. X, and propose how it can be used to test the physics we describe here experimentally, using the absorption spectrum of the system. We conclude our manuscript with the discussion in Sec. XI.

II. ZERO MODES IN BCS HAMILTONIANS MODULO SYMMETRY MANDATED DEGENERACIES

The most general BCS (Ref. 25) Hamiltonian has the form

$$\mathcal{H}_{\mathrm{BCS}} = \sum_{ab} \left[f_a^\dagger h_{ab} f_b - \frac{1}{2} f_a \Delta_{ab} f_b - \frac{1}{2} f_b^\dagger \Delta_{ab}^* f_a^\dagger \right], \qquad (1)$$

where a,b are generalized coordinates, and may include spin, position, and any other degree of freedom one can imagine. The fermionic operators f_a satisfy standard anticommutation relations. The operator h is Hermitian, and the pairing function must be antisymmetric in the generalized coordinates $\Delta_{ab}=-\Delta_{ba}$. A Bogoliubov transformation $\gamma_E^\dagger = \Sigma_a [u_{Ea} f_a^\dagger + v_{Ea} f_a]$ diagonalizes this quadratic Hamiltonian. From the eigenstate equations $[\mathcal{H}_{\mathrm{BCS}}, \gamma_E^\dagger] = E\gamma_E^\dagger$ the BdG equations are derived,

$$\begin{pmatrix} h & \Delta \\ \Delta^\dagger & -h^T \end{pmatrix} \cdot \psi = E\psi, \qquad (2)$$

where $\psi=(u_a,v_a)$ (we drop the E index to avoid clutter). The BdG equations are then simply the eigenvalue problem $\mathcal{H}_{\mathrm{BdG}}\psi=E\psi$, in terms of the BdG Hamiltonian $\mathcal{H}_{\mathrm{BdG}}$. This operator has the symmetry $\omega^x \mathcal{H}_{\mathrm{BdG}} \omega^x = -\mathcal{H}_{\mathrm{BdG}}^*$, where ω^x is the x-Pauli matrix in the so-called Nambu spinor basis $\omega^{x,y,z}$ (see Table I), acting on the (u,v) components of $\mathcal{H}_{\mathrm{BdG}}$. The Nambu spinor obeying $\omega^z\psi=+\psi$ corresponds to a pure fermion $(v_a=0)$, while $\omega^z\psi=-\psi$ corresponds to a pure hole $(u_a=0)$. This relation tells us that given an eigenvector ψ with eigenvalue E, $\omega^x\psi^*$ will also be an eigenvector with the eigenvalue $-E$. The matrix eigenvalue Eq. (2) can indeed

TABLE I. Pauli-matrix sets.

Spinor type	Nambu spinor	Spin spinor	Sublattice spinor	Dirac valley spinor
Pauli matrices	$\omega^{x,y,z}$	$\sigma^{x,y,z}$	$\eta^{x,y,z}$	$\tau^{x,y,z}$
Index variables		α,β	μ,ν	A,B
Index values		$\uparrow,\downarrow$	1,2	R,L

yield both positive and negative eigenvalues; however it is important to note that in this formulation of the BdG equations, the operators $\gamma_E^\dagger=\gamma_{-E}$, and so these pairs of $\pm E$ energy states are *not* independent.[2] This is a consequence of the doubling of the number of degrees of freedom in Eq. (1).[26]

The BCS ground state is a state that is annihilated by $\gamma_E|\mathrm{BCS}\rangle$ for $E>0$, and by $\gamma_E^\dagger|\mathrm{BCS}\rangle$ for $E<0$, which really are the same set of operators. Naively, one would be tempted to think of the ground state as a fermi sea of quasiparticle levels, all occupied below the Fermi level $E<0$, and all unoccupied for levels above $E>0$. However, as we see here, the "hole" $\gamma_{-E}|\mathrm{BCS}\rangle$ and particle $\gamma_E^\dagger|\mathrm{BCS}\rangle$ excitations (here $E>0$) are in fact the *same*, and so the BCS ground state should *not* be thought of as a filled Fermi sea of Bogoliubov quasiparticles. In the physical interpretation of the spectrum of the BdG equations, only the eigenvectors with energies $E\geq 0$ should be understood as wave functions of physical excitations.

Despite the subtleties of the physical interpretation of the BdG equations in this form, the purely mathematical analysis of them as an eigenvalue problem is extremely useful in identifying topologically protected zero modes. The BdG Hamiltonian [the matrix-operator of Eq. (2)] has a spectrum with $\pm E$ energy pairs. For zero modes ($E=0$), if some perturbation to the BdG matrix operator were to cause the zero-mode eigenstate to acquire nonzero energy, there would have to be another zero-mode eigenstate acquiring the *opposite* nonzero energy. The Atiyah-Singer index theorem[27] tells us that the number of solutions to an eigenvalue problem cannot be changed when deforming the operator continuously. Plainly put, new eigenstates cannot appear out of thin air—they must be deformations of eigenstates of the unperturbed system. Therefore, if the zero modes appear in pairs, they can in principle split. However, if the number of zero modes is *odd*, then at least one zero mode cannot be split by any physical perturbation [those that preserve the general form of BCS Hamiltonian (1)], and it is thus topologically robust.

The most celebrated example of this is the p_x+ip_y state, in which there is *one* zero mode bound to a (unit-vorticity) vortex[1] core, and so it is topologically protected. If the BdG matrix-operator spectrum has some degeneracy mandated by symmetries of the system that are conserved by physical perturbations, then the same degeneracy must hold. It then suffices for the zero modes to have an odd number modulo the minimal degeneracy mandated by the symmetries of the system in order to be topologically protected—deviation from zero energy would split the zero modes in half, and the degeneracy protected by the symmetry would be violated. It is however important to realize that if the deformation breaks the symmetries dictating the degeneracy of the entire spectrum, the zero modes may split. The zero modes are therefore protected by the *combination* of symmetry and topological protection.

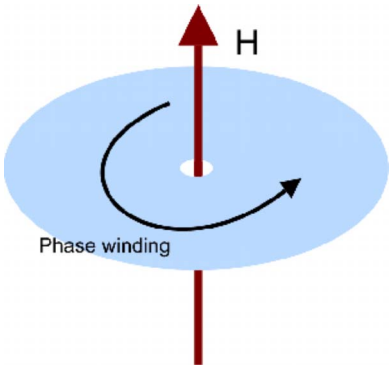

FIG. 1. (Color online) The punctured infinite plane geometry, with a magnetic flux threaded through the puncture (a vortex).

III. EQUIVALENCE OF VORTEX BOUND STATES AND EDGE STATES

In this section we will argue that quite generally the vortex-core bound zero-mode states should be *identified* with zero-mode edge states, in condensate phases. The connection between the presence of zero modes at vortex cores and at sample edges has been previously examined in the context of p_x+ip_y condensates of quadratic-dispersion fermions.[1,16]

Consider the infinite plane with the order-parameter amplitude nonzero and radially uniform only in the range $r>L$. Note that in the case of the p_x+ip_y condensate the order parameter has the form[1] $\{\Delta,\partial_x+i\partial_y\}$, and we refer to Δ as the condensate amplitude. The order parameter will include a phase winding $\Delta=|\Delta|e^{im\phi}$ (here and throughout this section, m is an integer), so that the region $r<L$ at the disk center models a vortex core. A state bound to the vortex core will have a radial profile for the wave function that is decaying exponentially $\sim e^{-\lambda r}$ in the superconducting region $r>L$. In order for the wave function to be normalizable in the $r\to 0$ limit as well, the wave-function amplitude must have the form $|\psi|\sim r^\nu$ with $\nu>-1$, in this limit. For $\nu=-1$, the wave-function norm $\int_0^a|\psi|^2rdr\sim\log\frac{a}{\epsilon}|_{\epsilon\to 0}$ diverges logarithmically. We have, therefore, uncovered another boundary condition on the wave function—ψr must vanish at $r=0$. Since bound-state zero modes should not be sensitive to the detailed boundary condition inside the vortex core,[1] the $r=0$ point can then be mapped onto a hard wall of a small radius $r=\delta$, on which $\psi r=0$, and therefore $\psi=0$ on this wall. An even simpler model of the vortex is obtained when we identify $\delta=L$. The geometry then consists of a punctured infinite disk (see Fig. 1), with the condensate order-parameter amplitude having uniform magnitude, and including a phase winding.

The geometry of the punctured infinite plane can be continuously deformed into a semi-infinite cylinder geometry (see Fig. 2), with radius L. Taking $L\to\infty$ then turns the geometry into the semi-infinite plane (Fig. 3). The boundary condition at $r=L$ corresponds now to a hard wall sample edge $\psi|_{\mathrm{wall}}=0$. The radial exponentially decaying solution of

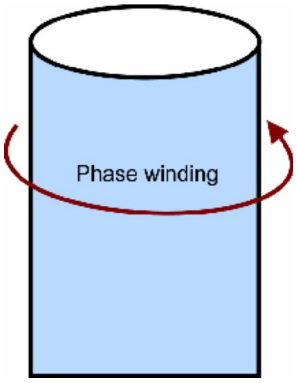

FIG. 2. (Color online) The semi-infinite cylinder geometry, topologically equivalent to the punctured infinite plane. There is a phase winding around the cylinder, corresponding to the phase winding of the vortex.

the punctured infinite plane geometry will deform into an exponentially decaying solution in the direction perpendicular to the edge (see Fig. 3), and the decay length will remain the *same* in both geometries (in terms of the physical length scales in the system).

The phase winding can be ignored in the formal limit $L \to \infty$, but must be taken into account when considering a finite size of the plane. The smooth deformation we employed to map between the vortex and an edge will also map $\Delta = |\Delta| e^{im\phi} \to \Delta = |\Delta| e^{im2\pi \frac{y}{L}}$. The phase winding in the order parameter will change the bound-state wave functions qualitatively. When going from y to $y+L$ we will pickup the requisite phase of $2\pi m$.

With the insight from the last section, it is now clear that modulo symmetries that are not related to position space the mapping we have described here *identifies* the vortex-core topological zero modes and topological zero-mode edge states. Furthermore, we may conclude that showing the existence of one implies the existence of the other. Indeed, for the $p_x + ip_y$ superconducting phase it is known[1,15,16] that zero-mode edge states exist in the presence of a vortex.

It is instructive to examine how the momentum quantization evolves when mapping between the vortex and the edge geometries. Consider the semiclassical limit introduced in Ref. 24, where the quantization of angular/linear momenta

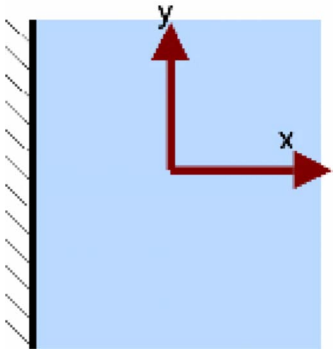

FIG. 3. (Color online) The semi-infinite plane geometry, topologically equivalent to the punctured infinite plane.

can be inferred from a Bohr-Sommerfeld quantization rule of the classical orbits,

$$2\pi\ell\hbar = \oint \mathbf{p} \cdot d\mathbf{x} + \frac{\hbar}{2} \oint \mathcal{A}(\hat{n}) \cdot d\hat{n}, \tag{3}$$

where here and in what follows ℓ is integer, and the second integral on the right-hand side (RHS) is the Berry phase traced by the (classical) Nambu vector $\hat{n}$. Note that as opposed to Ref. 24, we do not transform to the London gauge. This is the result for a single band of quadratically dispersing fermions, and we assume that a similar quantization rule will appear when taking a similar semiclassical limit of the more general problem. In particular

$$2\pi\ell\hbar = \oint \mathbf{p} \cdot d\mathbf{x} + \text{topologically invariant terms} \ldots . \tag{4}$$

Then in the process of deforming from the vortex to the edge, only the first term on the RHS changes. For a rotationally symmetric system, if the angular momentum of the vortex-core bound states is quantized $Rp = \hbar(\ell + \gamma)$ $(0 \leq \gamma < 1)$, then the linear momentum for the edge states will be quantized as $q = \frac{2\pi\hbar}{L}(\ell + \gamma)$ (where $L = 2\pi R$ is as before, the system size in the direction parallel to the edge).

Typically, the edge state energies $E \sim q$ at low momenta/energy, and so we will need $\gamma = 0$ or integer angular-momentum states in the vortex core in order to support zero modes.

IV. CONDENSATE PHASES

In this section we briefly present the variety of condensate phases we will be examining in this manuscript. We begin by considering a simple model of fermions on the honeycomb lattice, either spinless or including spin. We include nearest-neighbor hopping (of strength t) and fermion density-density interactions

$$\mathcal{H} = -t \sum_{\langle ij \rangle \alpha} f^\dagger_{i\alpha} f_{j\alpha} + \mu \sum_{j\alpha} f^\dagger_{j\alpha} f_{j\alpha} + \sum_{ij,\alpha\beta} f^\dagger_{i\alpha} f_{i\alpha} V^{\alpha\beta}_{ij} f^\dagger_{j\beta} f_{j\beta}, \tag{5}$$

where $f_{j\alpha}$ are the bare fermionic operators. The indices i,j run over the sites of the honeycomb lattice, and the greek letters $\alpha, \beta = \uparrow, \downarrow$ denote the spin indices. We point out that we neglect the gauge field in all our calculations. For spinless fermions, the indices α, β should be dropped. The interaction matrix is symmetric $V^{\alpha\beta}_{ij} = V^{\beta\alpha}_{ji}$, and is chosen such that $V^{\alpha\alpha}_{ii} = 0$ so that μ indeed will be the Fermi energy. Throughout this manuscript we will assume we are in the weak-interaction limit $t \gg V_{ij}$ so that BCS mean-field theory is applicable.

A. Order parameters

An order parameter for off-diagonal long-range order can be chosen as $\Delta^{\alpha\beta}_{ij} = -2V^{\alpha\beta}_{ij} \langle (f_{i\alpha} f_{j\beta})^\dagger \rangle$ and must be antisymmetric $\Delta^{\alpha\beta}_{ij} = -\Delta^{\beta\alpha}_{ji}$. For spinless fermions, or spin-triplet (Δ symmetric in spin indices) condensates, the order parameter is antisymmetric in the lattice sites, and *must* break parity (the

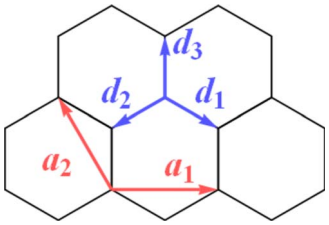

FIG. 4. (Color online) Conventions for the honeycomb lattice. The (blue) vectors marked $d_{1,2,3}$ represent the nearest-neighbor vectors from sublattice 1 to sublattice 2, and the (red) vectors $a_{1,2}$ mark the Bravais lattice vectors. In our conventions, the nearest-neighbor distance is set to 1.

order parameter becomes antisymmetric in swapping the i,j indices). A mean-field BCS Hamiltonian can then be obtained,

$$\mathcal{H}_{\mathrm{BCS}} = -t\sum_{\langle ij\rangle\alpha} f^{\dagger}_{i\alpha}f_{j\alpha} + \mu\sum_{j\alpha} f^{\dagger}_{j\alpha}f_{j\alpha} - \frac{1}{2}\sum_{ij,\alpha\beta}[f_{i\alpha}f_{j\beta}\Delta^{\alpha\beta}_{ij} + h.c.]. \tag{6}$$

In momentum space the BCS mean-field Hamiltonian reads

$$\mathcal{H}_{\mathrm{BCS}} = \sum_{\mathbf{q}}\sum_{\mu\nu}\left[\sum_{\alpha} f^{\dagger}_{\mu\alpha}(\mathbf{q})(\mu\delta_{\mu\nu} - t\Gamma(\mathbf{q})_{\mu\nu})f_{\nu\alpha}(\mathbf{q}) - \frac{1}{2}\sum_{\alpha\beta}[f_{\mu\alpha}(\mathbf{q})\Delta^{\alpha\beta}_{\mu\nu}(\mathbf{q})f_{\nu\beta}(-\mathbf{q}) + h.c.]\right], \tag{7}$$

where $f_{\mu\alpha}(\mathbf{q})$ are the bare fermionic operators in momentum space, and we have introduced the matrix

$$\Gamma(\mathbf{q}) = \begin{pmatrix} 0 & \gamma(\mathbf{q}) \\ \gamma(\mathbf{q})^{*} & 0 \end{pmatrix}. \tag{8}$$

The indices $\mu,\nu=1,2$ denote the two triangular sublattices of the honeycomb lattice. Note that while we use μ for both a sublattice index, and for the chemical potential, it should be clear from context when μ is used for one or the other (specifically, whenever both appear in the same equation, the index μ is always a subscript). Furthermore, $\gamma(\mathbf{q}) = \sum_{\ell=1}^{3} e^{+i\mathbf{q}\cdot\mathbf{d}_\ell}$, where $\mathbf{d}_{1,2,3}$ are the three vectors from any given site in sublattice 1 to its three nearest neighbors on sublattice 2 (see Fig. 4 for an illustration of our conventions). Finally, momentum is summed over the first Brillouin zone.

For spinless fermions or spin-triplet condensates, the parity broken Δ_{ij} implies $\Delta^{\alpha\beta}_{\mu\nu}(\mathbf{q}) = -\Delta^{\alpha\beta}_{\nu\mu}(-\mathbf{q})$. We now turn to several condensate order parameters of interest.

First, we mention the spin-singlet condensate phases introduced in Ref. 21, which take the form $\Delta^{\alpha\beta}_{ij} = \Delta_{ij} i\sigma^{y}_{\alpha\beta}$. Here and elsewhere we will use the notation $\sigma^{x,y,z}$ for the spin Pauli matrices (see Table I). The function Δ_{ij} is then symmetric, and Uchoa *et al.*[21] took $\Delta_{ij} = \delta_{ij}\Delta_0$ for an s-wave order parameter, and $\Delta_{ij} = \Gamma_{ij}\frac{1}{2}\Delta_1$, where Γ_{ij} is the adjacency matrix for the honeycomb lattice (takes a value of 1 for nearest-neighbor sites, and zero otherwise). The Δ_1 order parameter mimics the structure of the tight-binding kinetic-energy term for the honeycomb lattice, $\Sigma_{\langle ij\rangle}\ldots = \frac{1}{2}\Sigma_{ij}\Gamma_{ij}\ldots$, and in fact the Fourier transform of $\frac{1}{2}\Gamma_{ij}$ is simply the matrix $\Gamma(\mathbf{q})$ of Eq. (8). As a result, near half filling just as the tight-binding term has two Dirac nodes, so does the order parameter Δ_1. The Δ_1 order parameter then has the approximate form of a p_x+ip_y order parameter.[21] It may be a bit surprising to find a p_x+ip_y pairing function in a spin-singlet condensate since it is then antisymmetric under both spin exchange and momentum inversion. However, the additional structure from the sublattice basis provides a third antisymmetric component of the pairing function that keeps the overall antisymmetry. It is important to emphasize at this point that this p_x+ip_y phase is gapped only when we are away from half filling ($\mu \neq 0$).

Now we turn to spinless/spin-triplet order parameters. It is most convenient to write the spin-triplet order parameter in the form $\Delta^{\alpha\beta}_{ij} = [i\sigma^{y}\vec{\sigma}\cdot\vec{d}_{ij}]_{\alpha\beta}$. Here the (three-component) vector is antisymmetric $\vec{d}_{ij} = -\vec{d}_{ji}$. Let us focus on a single component of the vector $\vec{d}_{ij}$, to simplify our analysis, and also because this is equivalent to the spinless fermion case. Let us denote this single component as Δ_{ij}, which is still antisymmetric. The Fourier transform of this pairing function is a matrix $\Delta_{\mu\nu}(\mathbf{q})$. The sublattice structure now mimics the behavior of the spin matrix structure, and can allow both sublattice spinor-singlet as well as triplet structures. We introduce a new set of Pauli matrices $\eta^{x,y,z}$ in the two-sublattice space (see Table I), and now the spinless fermion pairing function can be written in complete generality as $\Delta_{\mu\nu}(\mathbf{q}) = [i\eta^{y}\vec{\eta}\cdot\vec{\Delta}(\mathbf{q}) + i\eta^{y}\Delta_0(\mathbf{q})]_{\mu\nu}$. As mentioned earlier in this section, the order parameter for spinless fermions will satisfy $\Delta_{\mu\nu}(\mathbf{q}) = -\Delta_{\nu\mu}(-\mathbf{q})$, implying that $\Delta_0(\mathbf{q}) = \Delta_0(-\mathbf{q})$ and $\vec{\Delta}(\mathbf{q}) = -\vec{\Delta}(-\mathbf{q})$.

The simplest momentum structure in the order parameter $\Delta_{\mu\nu}(\mathbf{q})$ would be just a function uniform in momentum space. A valid antisymmetric s-wave order parameter for spinless fermion pairing is $\Delta_{\mu\nu}(\mathbf{q}) = \left(\begin{smallmatrix} 0 & -i\Delta_0 \\ i\Delta_0 & 0 \end{smallmatrix}\right) = \eta^{y}\Delta_0$. However, attempting to transform this order parameter back to real space reveals that it break the honeycomb lattice symmetries. Namely, the pairing function Δ_{ij} is nonzero only for i,j on different sublattices, and in the same unit cell. The other nearest-neighbors pairs of either i,j do not enjoy a pairing amplitude, and so discrete rotation symmetry is broken.

For an order parameter that is linear in momentum (at least in a continuum limit), and maintains all the symmetries of the honeycomb lattice (apart from the inversion symmetry, as mentioned above), we take Δ_{ij} nonvanishing only on nearest-neighbor links. We choose for the directed links from one sublattice to the other the value $\Delta_{ij} = \Delta_2$, and opposite for $\Delta_{ji} = -\Delta_2$. In momentum space, the order parameter yields

$$\Delta_{\mu\nu} = \Delta_2 \begin{pmatrix} 0 & \gamma(\mathbf{q}) \\ -\gamma(\mathbf{q})^{*} & 0 \end{pmatrix}_{\mu\nu}. \tag{9}$$

This pairing function can be conveniently rewritten as $\Delta_{\mu\nu} = \Delta_2\eta^{z}\Gamma(\mathbf{q})$. We note that this pairing function includes parts that are symmetric as well as antisymmetric in the sublattice space. This pairing function is a directed version of the link-pairing order parameter in Ref. 21, and similarly, when the fermions in the system are near half filling, a p_x+ip_y structure appears from the matrix $\Gamma(\mathbf{q})$, and the order parameter

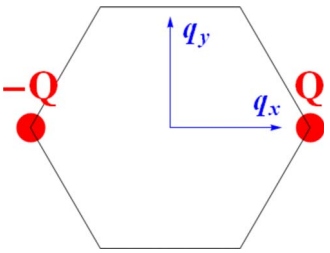

FIG. 5. (Color online) First Brillouin zone of the honeycomb lattice, showing the two Dirac node positions $\pm\mathbf{Q}$ (in red), and the main (x,y) axes indicated (in blue).

has the approximate symmetry of a p_x+ip_y order parameter.

With the spinless p_x+ip_y pairing, the bulk energy spectrum for the precise lattice model is found to be $E=\pm[(t^2+|\Delta_2|^2)|\gamma|^2+\mu^2\pm t|\gamma|\sqrt{|\Delta_2|^2(\gamma+c.c)^2+4\mu^2}]^{1/2}$ and it has nodes at the points $\mathbf{q}=p(1,\frac{1}{\sqrt{3}})$, where $p=\arccos(\frac{|\mu|}{2\sqrt{t^2-|\Delta_2|^2}}-\frac{1}{2})$, and symmetry-related points. These points satisfy γ *real*, and $|\gamma|^2=\frac{\mu^2}{t^2-|\Delta|^2}$. Regardless of where the Fermi surface is, the nodal points are near the Fermi surface defined by $|\gamma|^2=\frac{\mu^2}{t^2}$ since $|\Delta|\ll t$. A superconducting phase with nodes very close to the Fermi surface allows for bulk states below the momentum space averaged gap. Our analysis in the Appendix will indeed confirm this.

In the following sections we will perform an exhaustive analysis of the two spin-singlet-pairing phases to determine whether they allow topological zero modes. The analysis of the spinless phase we leave to the Appendix because this phase has gapless bulk excitations.

B. Continuum limit

Analyzing the bound states in a vortex or an edge is most easily done in a continuum limit of the lattice model. Here we will follow the conventions of Ref. 28, and work in the so-called "valley-isotropic" convention of the honeycomb lattice fermionic models near half filling. We demonstrate how this continuum limit is used on the BCS Hamiltonian[25] for the various condensate states we will consider here.

The Dirac nodes are a pair of points where $\gamma(\pm\mathbf{Q})=0$ (see Fig. 5 for illustration). In our conventions, the Dirac nodes are positioned at $\mathbf{Q}=(\frac{4\pi}{3\sqrt{3}},0)$ and $-\mathbf{Q}$. The fermi operators are expanded about these two nodes,[29] in the so-called valley-isotropic convention, and the two modes are identified as right (R) and left (L),

$$f_{\mu\alpha}(\mathbf{q}+\mathbf{Q})\approx\Pi\psi_{\mu\alpha R}(\mathbf{q}),$$

$$f_{\mu\alpha}(\mathbf{q}-\mathbf{Q})\approx\Pi i\eta^y_{\mu\nu}\psi_{\nu\alpha L}(\mathbf{q}). \tag{10}$$

Here Π is some normalization, and we have used the y-Pauli matrix η^y acting in the sublattice (μ,ν) spinor space, which was introduced in Sec. IV A.

In addition to the Nambu, spin, and sublattice spinor Pauli matrices, we now introduce a fourth set of Pauli matrices $\tau^{x,y,z}$ that act in the Dirac valley $(A,B=R,L)$ spinor space (see Table I). For clarity, from this point on, whenever it is convenient we will suppress indices which are being summed over.

We expand the kinetic energy about the two Dirac nodes, using $\gamma(\mathbf{q}\pm\mathbf{Q})\approx\mp\frac{3}{2}(p_x\mp ip_y)+\frac{3}{8}(p_x\pm ip_y)^2+\ldots$, to obtain

$$\Gamma(\mathbf{q}\pm\mathbf{Q})\approx\mp\frac{3}{2}(\eta^x q_x\pm\eta^y q_y)+\frac{3}{8}[\eta^x(q_x^2-q_y^2)\mp 2\eta^y q_x q_y]. \tag{11}$$

Organizing the expressions using the various Pauli-matrix sets we have introduced, and using the continuum Fourier transform

$$\psi_{\mu\alpha A}(\mathbf{q})=\int d^2\mathbf{x}e^{-i\mathbf{q}\cdot\mathbf{x}}\psi_{\mu\alpha A}(\mathbf{x}), \tag{12}$$

we derive a real-space continuum version of the kinetic energy

$$\mathcal{H}_{\text{kinetic}}=\int d^2\mathbf{x}\psi^\dagger\Big[\mu-iv(\vec{\eta}\cdot\nabla)+\frac{v}{4}\tau^z(\eta^x(\partial_x^2-\partial_y^2)-2\eta^y\partial_x\partial_y)\Big]\psi, \tag{13}$$

where $\vec{\eta}=\hat{x}\eta^x+\hat{y}\eta^y$ and $v=t\frac{3}{2}$.

At this point we observe that keeping only the linear derivatives, we obtain the celebrated Dirac operator, and at that level of approximation the Kinetic term has an SU(2) symmetry of valley spinor $(\tau^{x,y,z})$ rotations, in addition to the spin SU(2) symmetry. The last term is a quadratic correction to the Dirac operator that explicitly *breaks* the Dirac spinor SU(2) invariance, reducing it to a U(1) symmetry of rotations about τ^z. This correction, while often ignored, will be examined in the calculations we perform here.

Next we turn to the pairing term in the BCS Hamiltonian. With the three pairing phases we outlined in Sec. IV A, and using the various Pauli matrices we defined to compactify the expressions, the lattice Hamiltonian pairing term is

$$\mathcal{H}_{\text{pairing}}=-\frac{1}{2}\sum_{\mathbf{q}}\{f(\mathbf{q})[i\sigma^y(\Delta_0+\Delta_1\Gamma(\mathbf{q}))+\Delta_2\eta^z\Gamma(\mathbf{q})]f(-\mathbf{q})+h.c.\}. \tag{14}$$

In the continuum limit, we approximate BCS off-diagonal terms in the following manner:

$$\begin{aligned}\sum_{\mathbf{p}}f(\mathbf{p})M(\mathbf{p})f(-\mathbf{p})&\approx\sum_{\mathbf{q}}[f(\mathbf{q}+\mathbf{Q})M(\mathbf{q}+\mathbf{Q})f(-\mathbf{q}-\mathbf{Q})\\&\quad+f(\mathbf{q}-\mathbf{Q})M(\mathbf{q}-\mathbf{Q})f(-\mathbf{q}+\mathbf{Q})]\\&\approx\Pi^2\sum_{\mathbf{q}}[\psi_R(\mathbf{q})M(\mathbf{q}+\mathbf{Q})i\eta^y\psi_L(-\mathbf{q})\\&\quad+\psi_L(\mathbf{q})(-i)\eta^yM(\mathbf{q}-\mathbf{Q})\psi_R(-\mathbf{q})],\end{aligned} \tag{15}$$

where $M(\mathbf{p})$ is the pairing function. In our case, the pairing function from Eq. (14) is most conveniently cast as

$$M(\mathbf{p})=i\sigma^y(\Delta_0+\Delta_1\Gamma)+\Delta_2\eta^z\Gamma. \tag{16}$$

Using the lowest order in expansion (11), the identity $\eta^y(\vec{\eta}^*\cdot\mathbf{q})\eta^y=-(\vec{\eta}\cdot\mathbf{q})$, and absorbing a factor of $\frac{3}{2}$ into both $\Delta_{1,2}$, we find

$$M(\mathbf{q}+\mathbf{Q})i\eta^y \approx [i\sigma^y(\Delta_0 - \Delta_1(\vec{\eta}\cdot\mathbf{q})) - \Delta_2\eta^z\vec{\eta}\cdot\mathbf{q}]i\eta^y - i\eta^y M(\mathbf{q}-\mathbf{Q}) \approx [i\sigma^y(-\Delta_0 + \Delta_1(\vec{\eta}\cdot\mathbf{q})) - \Delta_2\eta^z\vec{\eta}\cdot\mathbf{q}]i\eta^y. \quad (17)$$

Combining these results, we find the pairing term in the Hamiltonian becomes in the continuum limit

$$\mathcal{H}_{\text{pairing}} = -\frac{1}{2}\sum_{\mathbf{q}}\{\psi(\mathbf{q})[i\sigma^y\tau^y\eta^y\Delta_0 - \sigma^y\tau^y\Delta_1(\vec{\eta}\cdot\mathbf{q})\eta^y + \tau^x\Delta_2\eta^z(\vec{\eta}\cdot\mathbf{q})\eta^y]\psi(-\mathbf{q}) + h.c.\}. \quad (18)$$

In order to be able to take slowly spatially varying order-parameter amplitudes ($\Delta_{0,1,2}$), we need to reorganize the pairing term in real space as

$$\mathcal{H}_{\text{pairing}} = -\frac{1}{2}\int_{\mathbf{x}}\left\{\psi\left[i\sigma^y\tau^y\eta^y\Delta_0 - i\sigma^y\tau^y\frac{1}{2}\{\Delta_1,(\vec{\eta}\cdot\nabla)\eta^y\} + i\tau^x\frac{1}{2}\{\Delta_2,\eta^z(\vec{\eta}\cdot\nabla)\eta^y\}\right]\psi + h.c.\right\}, \quad (19)$$

where all the operators ψ are function of $\mathbf{x}$, and $\{..,..\}$ denotes the anticommutator.

C. Bogoliubov-de-Gennes equations

With the final continuum forms of the kinetic [Eq. (13)] and pairing [Eq. (19)] terms of the BCS Hamiltonian, we can derive the BdG equations following the details of Sec. II. The BdG equations for the phases we examine in this manuscript take the form

$$\mathcal{H}_{\text{BdG}}\cdot\begin{pmatrix}u\\v\end{pmatrix} = E\begin{pmatrix}u\\v\end{pmatrix}, \quad (20)$$

where $\mathcal{H}_{\text{BdG}}=\mathcal{H}_0+\mathcal{H}_1+\mathcal{H}_2+\mathcal{H}_3+\mathcal{H}_4$. Here the kinetic term is

$$\mathcal{H}_0 = \begin{pmatrix}[\mu - iv(\vec{\eta}\cdot\nabla)] & 0\\ 0 & -[\mu + iv(\vec{\eta}^*\cdot\nabla)]\end{pmatrix} = \mu\omega^z - iv(\eta^x\partial_x + \eta^y\omega^z\partial_y) = \mu\omega^z - iv\hat{D}, \quad (21)$$

where we have introduced $\hat{D}=(\eta^x\partial_x+\eta^y\omega^z\partial_y)$. The singlet s-wave pairing term is

$$\mathcal{H}_1 = \begin{pmatrix}0 & +i\Delta_0\eta^y\sigma^y\tau^y\\ -i\Delta_0^*\eta^y\sigma^y\tau^y & 0\end{pmatrix} = -\eta^y\sigma^y\tau^y|\Delta_0|\omega^x e^{i\phi_0\omega_z} = -\eta^y\sigma^y\tau^y|\Delta_0|[\omega^x\cos(\phi_0)+\omega^y\sin(\phi_0)], \quad (22)$$

where $-\phi_0$ is the phase of $-i\Delta_0$. The singlet p_x+ip_y pairing term is

$$\mathcal{H}_2 = \begin{pmatrix}0 & -i\sigma^y\tau^y\frac{1}{2}\{\Delta_1,(\vec{\eta}\cdot\nabla)\eta^y\}\\ -i\sigma^y\tau^y\frac{1}{2}\{\Delta_1^*,\eta^y(\vec{\eta}\cdot\nabla)\} & 0\end{pmatrix} = -\frac{1}{2}\sigma^y\tau^y\omega^x\eta^y\{|\Delta_1|\exp^{+i\phi_1\omega_z},\hat{D}\}, \quad (23)$$

where $-\phi_1$ is the phase of $-i\Delta_1$. Finally, the spinless p_x+ip_y pairing term is

$$\mathcal{H}_3 = \begin{pmatrix}0 & i\tau^x\frac{1}{2}\{\Delta_2,\eta^z(\vec{\eta}\cdot\nabla)\eta^y\}\\ i\tau^x\frac{1}{2}\{\Delta_2^*,\eta^y(\vec{\eta}\cdot\nabla)\eta^z\} & 0\end{pmatrix} = \frac{i}{2}\tau^x\eta^x\omega^x\{|\Delta_2|e^{+i\phi_2\omega^z},\hat{D}\}, \quad (24)$$

where $-\phi_2$ is the phase of $i\Delta_2$. Finally, the quadratic correction to the kinetic term is

$$\mathcal{H}_4 = \frac{v}{4}\tau^z[\omega^z\eta^x(\partial_x^2-\partial_y^2) - 2\eta^y\partial_x\partial_y] = \frac{v}{4}\tau^z\hat{D}^*\hat{D}\omega^z\eta^x. \quad (25)$$

This concludes our derivation of the BdG continuum equations, which we will now investigate in a variety of geometries, to determine whether topological zero modes appear.

D. Quantization rule

In Sec. III we pointed out how the momentum quantization evolves when mapping between the vortex and edge geometries. We assumed that the Bohr-Sommerfeld quantization rule takes on the form of Eq. (4). In this short subsection we will briefly deduce what the quantization rule is for the specific cases we consider in this section.

In the effective continuum theory, the Dirac valley spinor degree of freedom is independent of the real-space position degree of freedom. Therefore, the only significant difference between the BdG Hamiltonians we deal with here and those dealt with in Ref. 24 are the appearance of additional spinor structures—the spin, sublattice, and Dirac valley spinors. Following the semiclassical derivation of Ref. 24, we can use a coherent-state representation of spin $\frac{1}{2}$ not only for the Nambu spinor, but also for the two other spinors as well. We introduce classical unit vectors for each one of the spinors $\hat{n}$ for the Nambu spinor, $\hat{h}$ for the sublattice spinor, and $\hat{t}$ for the Dirac valley spinor. For the cases where our fermions have spin, there is also a spin degree of freedom, for which we use $\hat{s}$ for the coherent-state representation of the spin. The path-integral formulation will include a Berry phase for each one of the unit vectors, so

$$S_B = \oint\mathbf{p}\cdot d\mathbf{x} + \frac{\hbar}{2}\oint\mathcal{A}_\omega(\hat{n})\cdot d\hat{n} + \frac{\hbar}{2}\oint\mathcal{A}_\sigma(\hat{s})\cdot d\hat{s} + \frac{\hbar}{2}\oint\mathcal{A}_\eta(\hat{h})\cdot d\hat{h} + \frac{\hbar}{2}\oint\mathcal{A}_\tau(\hat{t})\cdot d\hat{t}. \quad (26)$$

For the spinless case, the spin Berry phase term will be absent.

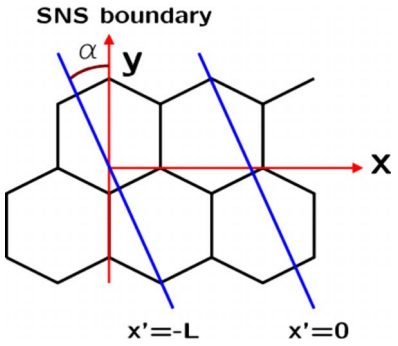

FIG. 6. (Color online) SNS junction on the background of the honeycomb lattice. Our conventions are that the SNS boundaries are at an angle α with the armchair y-direction in our conventions.

Finally, following Appendix C of Ref. 24, the Bohr-Sommerfeld quantization rule will be of the form $S_B=2\pi(\ell+\gamma)\hbar$ (the γ part coming from the order-parameter phase winding). We find therefore, that indeed in the cases we consider here, the Bohr-Sommerfeld quantization rule takes on the form of Eq. (4).

V. SNS JUNCTIONS

Perhaps the simplest indication of whether topological zero modes can exist in condensate systems is when considering SNS (superconducting-normal-superconducting) junctions.[24] In this section we will explore the spectrum of states bound to an SNS junction in the various condensate phases we mentioned in the previous section. This will serve a first step toward determining in which of these phases zero modes may appear.

The SNS junction is modeled as an infinite strip of width L in the continuum limit, where the pairing function vanishes (see Fig. 6). On the two sides of the strip are condensate regions, with a uniform pairing function, with a relative U(1) phase ϕ. For the SNS junction we have the pairing function

$$\Delta(x)=\begin{cases}\Delta e^{i\phi}, & x<-L\\ 0, & -L<x<0\\ \Delta, & 0<x,\end{cases} \tag{27}$$

where x is the coordinate in the direction perpendicular to the SNS junction walls.

A. Singlet *s*-wave condensate

Combining the kinetic energy [Eq. (21)] and s-wave pairing terms [Eq. (22)] the BdG equation for the s-wave condensate takes the form

$$\mathcal{H}_{\mathrm{BdG}}\psi=E\psi=\{\mu\omega^z-iv\hat{D}-\Delta[\omega^x\cos(\phi)+\omega^y\sin(\phi)]\eta^y\tau^y\sigma^y\}\psi, \tag{28}$$

where ϕ is the U(1) phase of the order parameter, and to avoid clutter we have dropped the 0 subscript from both the phase and order-parameter magnitude. It is convenient to work in the London gauge—we use a unitary transformation $\mathcal{O}=e^{-i(\phi/2)\omega^z}$ in order to rotate the phase $\phi\to 0$.

We are free to choose ψ to be eigenstates of τ^y,σ^y, such that $\tau^y\sigma^y\to\tau\sigma$. This fourfold degeneracy applies to the entire quasiparticle energy spectrum. We note here that the explicit appearance of τ^y,σ^y is misleading because the BCS Hamiltonian in this phase is in fact SU(2) invariant for *both* the spin and Dirac spinors. It is perhaps more appropriate to write $\sigma^y\tau^y=-\epsilon_\tau\epsilon_\sigma$ a product of the two totally antisymmetric 2×2 tensors in the spin and Dirac spinor space. The SU(2) invariance in both these spinor spaces then becomes evident (these appear in the pairing terms of the Hamiltonian). Further assuming that the SNS junction is aligned with a armchair line of the honeycomb lattice (y direction in our conventions—see Fig. 6) and that ψ only varies in the x direction, which we are allowed to assume in a y-infinite system, we find the BdG Hamiltonian reduces to

$$\mathcal{H}_{\mathrm{BdG}}=[\mu\omega^z-iv\eta^x\partial_x-\Delta\omega^x\eta^y\tau\sigma]. \tag{29}$$

Apart from the expected (see Sec. II) symmetry $\omega^x\mathcal{H}_{\mathrm{BdG}}\omega^x=-\mathcal{H}^*_{\mathrm{BdG}}$ it is also easy to show that $\eta^x\omega^z\mathcal{H}_{\mathrm{BdG}}\eta^x\omega^z=\mathcal{H}_{\mathrm{BdG}}$. This relation is special for y-independent states (once y variation is allowed this is no longer a symmetry of the Hamiltonian). The additional symmetry will yield a further double degeneracy of the spectrum, so we expect every energy level to be eightfold degenerate. The eigenstates of Eq. (29) obey

$$\partial_x\psi=A\psi=\frac{1}{iv}\eta^x[\mu\omega^z-E-\Delta\omega^x\eta^y\tau\sigma]\psi. \tag{30}$$

The matrix A is then diagonalized, using some (x-independent) similarity transformation U, and we find it has four eigenvalues

$$U^{-1}\cdot A\cdot U=\frac{1}{v}\mathrm{Diagonal}(-\sqrt{\Delta^2-E^2}+i\mu,-\sqrt{\Delta^2-E^2}-i\mu,+\sqrt{\Delta^2-E^2}+i\mu,+\sqrt{\Delta^2-E^2}-i\mu). \tag{31}$$

The diagonalizing transformation is

$$U=\begin{pmatrix}\alpha+iE & iE-\alpha & iE-\alpha & \alpha+iE\\ -\alpha-iE & iE-\alpha & \alpha-iE & \alpha+iE\\ \Delta\sigma\tau & -\Delta\sigma\tau & \Delta\sigma\tau & -\Delta\sigma\tau\\ \Delta\sigma\tau & \Delta\sigma\tau & \Delta\sigma\tau & \Delta\sigma\tau\end{pmatrix}, \tag{32}$$

where $\alpha=\sqrt{\Delta^2-E^2}$. When considering energy levels well below the condensate gap $E\ll\Delta$ we have $\sqrt{\Delta^2-E^2}>0$. Therefore, for $x>0$ we have the normalizable solution

$$\psi(x)=U\cdot(e^{(-\sqrt{\Delta^2-E^2}+i\mu)\frac{x}{v}}a_1,e^{(-\sqrt{\Delta^2-E^2}-i\mu)\frac{x}{v}}a_2,0,0)^T. \tag{33}$$

For $x<-L$ we have the normalizable solution

$$\psi(x)=\mathcal{O}\cdot U\cdot(0,0,e^{(+\sqrt{\Delta^2-E^2}+i\mu)\frac{x}{v}}b_1,e^{(+\sqrt{\Delta^2-E^2}-i\mu)\frac{x}{v}}b_2)^T. \tag{34}$$

We must now solve for the wave function ψ in the normal region, and then match the wave function at the interfaces. For $-L<x<0$ the pairing function vanishes, in which case

$A=\frac{1}{iv}\eta^x(\mu\omega^z-E)$, and since all solutions are normalizable in this region, we can write

$$\psi(x)=e^{Ax}\psi(x=0). \tag{35}$$

Now we match the wave function at $x=0,-L$. This will yield a set of linear equations with the variables $a_{1,2},b_{1,2}$. It can then be recast as a matrix equation $B\cdot(a_1,a_2,b_1,b_2)^T=0$, and for a nontrivial solution, we require that $\mathrm{Det}(B)=0$. The equation for the determinant turns out to be

$$\frac{4\cos\left(\frac{2LE}{v}\right)E^2}{\Delta^2}+\frac{4\sqrt{\Delta^2-E^2}\sin\left(\frac{2LE}{v}\right)E}{\Delta^2}-2\cos\left(\frac{2LE}{v}\right)-2\cos(\phi)=0\ . \tag{36}$$

The condition Eq. (36) induces a quantization of the energy values. In particular, we can now investigate whether zero modes are possible. With $E=0$, Eq. (36) becomes $\cos(\phi)=-1$, which means only when the two superconducting slabs have a π phase difference does a zero-mode eigenstate appear. Furthermore, we can find the spectrum of low-energy states—we use the limit $E\ll\Delta$ to approximate Eq. (36) as $\cos(\frac{2LE}{v})+\cos(\phi)\approx 0$ which then yields

$$E\approx\frac{v}{2L}2\pi\left(n+\frac{1}{2}-\frac{\phi}{2\pi}\right). \tag{37}$$

We find the spectrum is evenly spaced, with a spacing $\delta E=\frac{v}{2L}2\pi$.

The zero-mode wave functions can also be found (from the null space of the matrix B, with $E=0$ and $\phi=\pi$). Including the τ and σ spinors we have been ignoring, $\chi_\tau=(1,i\tau)^T$ and $\chi_\sigma=(1,i\sigma)^T$ we find a total of eight solutions,

$$\psi_{\eta\sigma\tau}(x)=\psi_\eta(0)\otimes\chi_\tau\otimes\chi_\sigma e^{\eta\frac{ix\mu}{v}}\begin{cases}e^{+\frac{(x+L)\Delta}{v}}, & x<-L\\ 1, & -L<x<0\\ e^{-\frac{x\Delta}{v}}, & x>0,\end{cases} \tag{38}$$

where $\psi_\eta(0)=\mathcal{N}(\sigma\tau,-\eta\sigma\tau,1,\eta)^T$, $\eta=\pm 1$, and $\mathcal{N}$ is a normalization factor. Here, and elsewhere in this section, the column vector $\psi_\eta(0)$ has the entries $(u_1,u_2,v_1,v_2)^T$, where 1 and 2 are the sublattice indices. These two solutions are independent (even at half filling $\mu=0$), and in fact are also eigenstates of $\eta^z\omega^x\psi_{\eta\sigma\tau}=\sigma\tau\psi_{\eta\sigma\tau}$ and $\eta^x\omega^z\psi_{\eta\sigma\tau}=-\eta\psi_{\eta\sigma\tau}$. It is also evident that $\omega^x\psi^*_{\eta\sigma\tau}=\sigma\tau\psi_{-\eta,-\sigma,-\tau}$.

As mentioned in Sec. IV B, the honeycomb lattice tight-binding model in the continuum limit includes a quadratic derivative correction to Dirac operator (25). Since the degeneracy in $\tau=\pm 1$ stems from the SU(2) valley spinor symmetry, which is explicitly broken [and reduced to U(1)] by Eq. (25), we should investigate whether this term splits the eight zero modes we have found. This will be our first step in exploring whether the zero modes appear in the original lattice model. Since we are considering here y-independent states, the correction reduces to

$$\mathcal{H}_4=\frac{v}{4}\tau^z\omega^z\eta^x\partial_x^2. \tag{39}$$

The correction commutes with $\eta^x\omega^z$, and is spin SU(2) invariant, so the quantum numbers η and σ are conserved, so only τ can mix and a quadruple degeneracy of every energy level will still hold. A simple calculation yields that all the matrix elements between the zero modes induced by the correction vanish, and so this term does not split the zero modes, in this SNS geometry, with the armchair alignment.

So far we have only considered a very particular alignment of the SNS junction walls—the y direction in our conventions for the honeycomb lattice. Now we turn to investigate whether different orientations of the SNS junction behave different. Rotating the SNS junction counterclockwise by an angle α (see Fig. 6), and assuming the eigenstates only vary in the direction perpendicular to the SNS junction walls, which we denote by x', the only term that changes in Eq. (28) in the London gauge is

$$\hat{D}(\alpha)=[\cos(\alpha)\eta^x+\sin(\alpha)\omega^z\eta^y]\partial_{x'}=\eta^x e^{+i\alpha\omega^z\eta^z}\partial_{x'}. \tag{40}$$

It is easy to show that the unitary transformation $U(\alpha)=e^{-i(\alpha/2)\omega^z\eta^z}$ will rotate $\alpha\to 0$, mapping this problem directly onto the problem with the SNS junction parallel to the y direction $U(\alpha)^\dagger\mathcal{H}_{\mathrm{BdG}}(\alpha)U(\alpha)=\mathcal{H}_{\mathrm{BdG}}(\alpha=0)$. Furthermore, the symmetry $[\mathcal{H},\omega^z\eta^x]=0$ will simply be replaced by $[\mathcal{H}(\alpha),U(\alpha)\omega^z\eta^xU(\alpha)^\dagger]=0$. Thus, we conclude that the eigenvalue spectrum, at least when ignoring the quadratic correction to the kinetic energy, is completely independent of the SNS junction orientation, and will remain eightfold degenerate.

The quadratic correction to the kinetic energy with the SNS junction walls rotated takes the form

$$\mathcal{H}_4=\frac{v}{4}\tau^z(\hat{D}(\alpha)^*\hat{D}(\alpha))\omega^z\eta^x=\frac{v}{4}\tau^z e^{i2\alpha\omega^z\eta^z}\omega^z\eta^x\partial_{x'}^2. \tag{41}$$

Now we want to examine how the correction transforms under the unitary transformation that rotates $\alpha\to 0$ in $\mathcal{H}_{\mathrm{BdG}}(\alpha)$. We note first that all terms in $\mathcal{H}_4$ apart from the operator η^x remain invariant under this unitary transformation. The correction becomes

$$\begin{aligned}U^\dagger\mathcal{H}_4U&=\frac{v}{4}\tau^z e^{i2\alpha\omega^z\eta^z}\omega^z U^\dagger\eta^x U\partial_{x'}^2,\\&=\frac{v}{4}\tau^z[\cos(3\alpha)\eta^x\omega^z-\sin(3\alpha)\eta^y]\partial_{x'}^2.\end{aligned} \tag{42}$$

The emergence of the 3α factors may seem a bit surprising, but in fact this is a consequence of the underlying threefold rotation symmetry of the honeycomb lattice—the splitting is the same if we rotate the SNS junction by $2\pi/3$. The correction naturally reduces to Eq. (39) when $\alpha=0$. In fact, the first term above is precisely the $\alpha=0$ splitting matrix multiplied by the factor $\cos(3\alpha)$. Using this fact, we need only compute the matrix elements of the second term when projected onto the subspace of zero modes. The result is

$$\langle \psi_{\eta'\sigma'\tau'}|U^\dagger \mathcal{H}_4 U|\psi_{\eta\sigma\tau}\rangle = -\sin(3\alpha)\delta_{\sigma'\sigma}\eta^y_{\eta'\eta}\frac{\Delta^2}{8(v+L\Delta)}\left\{\tau^x_{\tau'\tau}\sin\left(\frac{2L\mu}{v}\right) + \tau^y_{\tau'\tau}\left[1+\cos\left(\frac{2L\mu}{v}\right)\right]\right\}, \quad (43)$$

In general the eigenvalues of this matrix will be nonvanishing (except for the special pathological cases $\frac{2L\mu}{v}=\pi$ and α an integer multiple of $\pi/3$), thus splitting the zero-mode energies.

To conclude this subsection, we have shown that in the SNS junction geometry, the honeycomb Dirac dispersion *s*-wave condensate can support topological zero modes, when an odd phase winding is present (the π phase difference between the condensate slabs). However, these zero modes split when we take into account quadratic corrections to the kinetic energy, which are intrinsically present in the honeycomb lattice. Only in the case where the junction walls are aligned as armchair boundaries in the honeycomb lattice ($\alpha=0$) do the zero modes remain unsplit by the quadratic correction.

B. Singlet $p+ip$ condensate

Now we turn to SNS junctions in the p_x+ip_y singlet phase. Our analysis will be very similar to that carried out in Sec. V A for the *s*-wave phase, and as such we will describe our calculations in much less detail. Here and throughout the remainder of our manuscript, we will assume $\mu>0$ for all of the p_x+ip_y phases since these are gapped only away from half filling, and since essentially the same result can be found for $\mu<0$ (due to the honeycomb particle-hole symmetry).

With a (piecewise) uniform pairing function, combining the kinetic energy [Eq. (21)] and the spin-singlet p_x+ip_y pairing terms [Eq. (23)] the BdG equation takes the form

$$\mathcal{H}_{\mathrm{BdG}}\psi = E\psi = \{\mu\omega^z - iv\hat{D} - \Delta[\omega^x\cos(\phi) + \omega^y\sin(\phi)]\eta^y\hat{D}\tau^y\sigma^y\}\psi, \quad (44)$$

where we have dropped the 1 subscript from both the order-parameter phase and magnitude to avoid clutter. As before we will work in the London gauge—the unitary transformation $\mathcal{O}=e^{-i(\phi/2)\omega^z}$ will rotate the phase $\phi\to 0$.

Given what we have learned about the significance of the SNS junction orientation in Sec. V A, we begin by briefly addressing this point. As in the *s*-wave case, we assume the angle between the SNS boundaries and the *y* axis is α, and consider eigenstates with spatial variation only in the direction perpendicular to the SNS boundaries. We use the same unitary transformation $U(\alpha)$ to rotate $\alpha\to 0$ in the kinetic energy. The pairing function now includes $\hat{D}$, which is also rotated to its $\alpha=0$ value, and all the other operators remain invariant. Choosing in addition eigenstates of τ^y,σ^y, the BdG Hamiltonian then reduces to

$$\mathcal{H}_{\mathrm{BdG}} = [\mu\omega^z - iv\,\eta^x\partial_x + i\Delta\omega^x\eta^z\tau\sigma\partial_x]. \quad (45)$$

At this point we will note that the BdG Hamiltonian we obtain here, just as its *s*-wave counterpart, has an extra symmetry $[\mathcal{H}_{\mathrm{BdG}},\eta^x\omega^z]=0$. As a result, we expect the spectrum to be eightfold degenerate.

Following the same procedure elaborated in Sec. V A, we find the energy quantization condition in the SNS junction to be

$$0 = \frac{2}{\Delta^2(E-\mu)^2}\left[-(E^2-\mu^2)\cos(\phi)\Delta^2 - ((E^2-\mu^2)\Delta^2 + 2v^2E^2)\cos\left(\frac{2LE}{v}\right) + 2ivE\sqrt{(E^2-\mu^2)\Delta^2+v^2E^2}\,\sin\left(\frac{2LE}{v}\right)\right]. \quad (46)$$

For low energies $E\ll\Delta$ this reduces to $\cos(\phi)+\cos(\frac{2LE}{v})$ and we obtain the low-energy spectrum

$$E = \frac{v\pi}{L}\left(n+\frac{1}{2}-\frac{\phi}{2\pi}\right), \quad (47)$$

identical to the spectrum we found for the *s*-wave phase, and including zero modes, only when $\phi=\pi$.

Using the same conventions we used for the *s*-wave case, the zero-mode wave functions we find, when taking $\phi=\pi$, are

$$\psi_{\eta\sigma\tau}(x) = \psi_\eta(0)\otimes\chi_\tau\otimes\chi_\sigma e^{\eta(ix\mu/v)} \times\begin{cases} e^{(L+x)\Delta\mu/v(v+i\eta\Delta)}, & x<-L \\ 1, & -L<x<0 \\ e^{-x\Delta\mu/v(v-i\eta\Delta)}, & x>0, \end{cases} \quad (48)$$

where $\psi_\eta(0)=\mathcal{N}(-i\sigma\tau, i\eta\sigma\tau, 1, \eta)^T$ and $\mathcal{N}$ is a normalization factor. Quite similarly to the *s*-wave zero modes, these solutions are eigenstates of $\eta^x\omega^z\psi_{\eta\sigma\tau}=-\eta\psi_{\eta\sigma\tau}$ and of $\eta^z\omega^y\psi_{\eta\sigma\tau}=\sigma\tau\psi_{\eta\sigma\tau}$. From the form of the solutions it is also clear that $\omega(\psi_{\eta\sigma\tau})^*=i\sigma\tau\psi_{-\eta,-\sigma,-\tau}$.

Finally we discuss the influence of the quadratic correction to the kinetic energy. Here the value of α is significant, and so we go straight to Eq. (42), and calculate the matrix elements in the zero-mode subspace. We find that all the matrix elements *vanish*, and so zero modes are not split to first order in the correction.

C. SNS junctions summary

To conclude this section exploring the SNS junction geometry, we recap the results of our calculations. For simplicity we have limited our discussion to wave functions uniform in the direction parallel to the walls. The spin-singlet *s*-wave phase supports zero modes only when $\alpha=0$ (armchair boundary), and otherwise does not possess zero modes, with splitting due to the quadratic correction to the kinetic energy. The spin-singlet p_x+ip_y phase supports zero modes (to first order in perturbation theory in the quadratic correction).

VI. EDGE STATES

In this section we will investigate the edge state spectrum of the various phases we are exploring in this article. For convenience we will consider an edge where the honeycomb

lattice abruptly ends, and assume the pairing function is uniform in space. We expect the bound states with low energy to appear with low momentum in the direction parallel to the edge (in the lattice model), and because of this one needs to be somewhat cautious when thinking about the continuum limit. For the armchair edge of the honeycomb lattice, the Dirac point momenta are perpendicular to the boundary, and so low transverse momentum can be well described even in the continuum limit. For a zigzag edge, the Dirac momenta $\mathbf{Q}$ are parallel to the edge, and so small momentum in the lattice model $\mathbf{p}=\mathbf{Q}+\mathbf{q}\approx 0$ parallel to this edge corresponds to momentum of order the Dirac momentum in the continuum theory $\mathbf{q}\approx -\mathbf{Q}$. Under these extreme conditions, the validity of the continuum limit approximation for the lattice model breaks down—the real momentum is quite far away from the Dirac point. We will, therefore, explore only the armchair edge in our present work (corresponding to $\alpha=0$ in Sec. V A and shown in Fig. 6).

A. Boundary conditions in the continuum limit of the honeycomb lattice

Since we are taking a continuum limit of lattice models on the honeycomb, we must study with some care how the boundary conditions must be taken in the continuum limit.

With our choice of the armchair edge, the boundary condition of the lattice wave function is that it must vanish on some line. The eigenstates of the system are in general the Bogoliubov quasiparticles, with creation operators

$$\gamma^\dagger = \sum_{\mu\alpha\mathbf{r}} [\tilde{u}_{\mu\alpha}(\mathbf{r}) f^\dagger_{\mu\alpha}(\mathbf{r}) + \tilde{v}_{\mu\alpha}(\mathbf{r}) f_{\mu\alpha}(\mathbf{r})], \tag{49}$$

and the boundary condition corresponds to $\tilde{u}=\tilde{v}=0$ at the system edge. We note here that our description applies to noncondensate system as well, by simply taking $\tilde{v}=0$ *everywhere*, in which case the Bogoliubov quasiparticles simply become modes of the fermi gas.

In the continuum limit we employ here, the Bogoliubov quasiparticles are

$$\gamma^\dagger = \sum_{\mu\alpha A} \int_{\mathbf{r}} [u_{\mu\alpha A}(\mathbf{r}) \psi^\dagger_{\mu\alpha A}(\mathbf{r}) + v_{\mu\alpha A}(\mathbf{r}) \psi_{\mu\alpha A}(\mathbf{r})]. \tag{50}$$

Changing to momentum space in both cases, and using the transformation Eq. (10), we identify

$$u_{\mu\alpha R}(\mathbf{q}) = \tilde{u}_{\mu\alpha}(\mathbf{q}+\mathbf{Q})\Pi,$$

$$u_{\mu\alpha L}(\mathbf{q}) = -i\eta^y_{\mu\nu}\tilde{u}_{\nu\alpha}(\mathbf{q}-\mathbf{Q})\Pi,$$

$$v_{\mu\alpha R}(\mathbf{q}) = \tilde{u}_{\mu\alpha}(\mathbf{q}+\mathbf{Q})\Pi,$$

$$v_{\mu\alpha L}(\mathbf{q}) = +i\eta^y_{\mu\nu}\tilde{u}_{\nu\alpha}(\mathbf{q}-\mathbf{Q})\Pi. \tag{51}$$

Using these relations we can identify the continuum limit approximation of $\tilde{u},\tilde{v}$. We find

$$\tilde{u}_{\mu\alpha}(\mathbf{r}) \approx \Pi[u_{\mu\alpha R} e^{+i\mathbf{Q}\cdot\mathbf{r}} + i\eta^y_{\mu\nu} u_{\nu\alpha L} e^{-i\mathbf{Q}\cdot\mathbf{r}}],$$

$$\tilde{v}_{\mu\alpha}(\mathbf{r}) \approx \Pi[v_{\mu\alpha R} e^{+i\mathbf{Q}\cdot\mathbf{r}} - i\eta^y_{\mu\nu} v_{\nu\alpha L} e^{-i\mathbf{Q}\cdot\mathbf{r}}]. \tag{52}$$

Next we will use this continuum approximation of the lattice wave function to explore how the boundary conditions translate in the continuum limit.

In our convention, the armchair edge can occur at the line $x=0$, and since we have $\mathbf{Q}=Q\hat{x}$, the lattice wave-function boundary condition translates into the condition

$$u_R = -i\eta^y u_L,$$

$$v_R = +i\eta^y v_L, \tag{53}$$

for the continuum wave function, at $x=0$. Using the various Pauli-matrix sets we have defined earlier in this manuscript, we can reorganize these conditions into the simple form

$$\omega^z \eta^y \tau^y \psi = \psi, \tag{54}$$

where $\psi=(u,v)$ (the continuum limit wave function). In what follows, we will assume the lattice occupies the $x>0$ semi-infinite plain, and use the boundary condition we have derived here. It is worth while noting that when dealing with noncondensate wave functions, where $\omega_z\psi=\pm\psi$, the boundary condition we have derived here simply reduces to the previously derived armchair boundary condition[30] in the conventions of Ref. 31, $\eta^y\tau^y\psi=\pm\psi$.

B. Singlet *s*-wave condensate

We now turn to explore the edge states in the honeycomb spin-singlet condensate *s*-wave phase. Starting from the BdG equations Eq. (28), we choose the order-parameter phase $\phi=0$, and solutions that are eigenstates of $\sigma^y\psi=\sigma\psi$ and $\tau^y\psi=\tau\psi$, in which case

$$[\mu\omega^z - iv(\eta^x\partial_x + \omega^z\eta^y\partial_y) - \omega^x\eta^y\tau\sigma\Delta]\psi = E\psi. \tag{55}$$

In the semi-infinite geometry, the system is still translationally invariant in the y direction, so we choose solutions of the form $\psi(x,y)=e^{iqy}\psi(x)$. The BdG equations then become

$$[\mu\omega^z - iv\eta^x\partial_x + vq\omega^z\eta^y - \omega^x\eta^y\tau\sigma\Delta]\psi(x) = E\psi(x). \tag{56}$$

Boundary condition (54) then requires $\omega^z\eta^y\psi(x=0)=\tau\psi(x=0)$.

The set of coupled ODEs can be solved in a manner very similar to the way we solved for the $x>0$ region of the SNS junction. we cast the equations in the form $\partial_x\psi=A\psi$, with the matrix A being independent of x. We diagonalize the matrix A with a similarity transformation that is x independent, and then keep those solutions that are exponentially decaying in $x>0$. In contrast to the SNS junction case, here we allow for a transverse momentum, and for this reason the calculations are somewhat more involved. These solutions can be written as

$$\psi_{\eta,\tau,\sigma} = \chi_\sigma \otimes \chi_\tau \otimes e^{-xF_\eta/v+iqy} \begin{pmatrix} \frac{\eta(\Delta^2+i\eta(B+iE\eta)(E-\mu))\sigma\tau}{2\Delta(B-i\eta\mu)} \\ -\frac{(B+iE\eta)\sigma\tau(qv+F_\eta)}{2\Delta(B-i\eta\mu)} \\ \frac{\eta(qv+F_\eta)}{2(B-i\eta\mu)} \\ \frac{1}{2} \end{pmatrix}, \tag{57}$$

where we have introduced $B=\sqrt{\Delta^2-E^2}$ and $F_\eta = \sqrt{(B-i\eta\mu)^2+(qv)^2}$, and $\eta=\pm 1$. The components of the four-vector above correspond to the wave-function amplitudes $(u_1,u_2,v_1,v_2)^T$, where 1 and 2 are the two sublattice indices. Throughout this section all four-component vectors will follow this convention.

Note that for small energy $E \ll \Delta$ we have $B \approx \Delta$, and then further assuming that the momentum is small $qv \ll \Delta$ yields $F_\eta \approx (\Delta - i\eta\mu)$, which gives the decay length scale we found for the SNS junctions (as well as for the vortex-core case, as we will see in the next section). At this level, before we impose the edge boundary conditions, we find we have eight solutions per energy E and transverse momentum q.

The general spin-eigenvalue solution that decays exponentially in $x>0$ is $\psi=\psi_{+1}a_{+1}+\psi_{-1}a_{-1}$. Now we will impose armchair wall boundary conditions (54) to this solution. The boundary conditions gives two linearly independent equations in the variables a_η. These equations can be cast in matrix form, and for a nontrivial solution $a_\eta \neq 0$ to exist, the determinant of the matrix must vanish. The resultant equation for the determinant is a quantization condition for the energies E. The precise form of this quantization rule is

$$0 = i\tau B^3 + E\mu(F_{-1}-F_1) - iB\{q^2\tau v^2 + q[\tau(F_{-1}+F_1)-2E]v - E(F_{-1}+F_1) + \tau(F_{-1}F_1-\mu^2)\}. \tag{58}$$

Considering low energies $E \ll \Delta$, and small momentum $qv \ll \Delta$, we can approximate the quantization condition to $[(E-qv\tau)\Delta^2+E\mu^2] \approx 0$ which yields

$$E \approx \tau \frac{qv\Delta^2}{\Delta^2+\mu^2}. \tag{59}$$

We find that zero modes exist for $q=0$. Next we will obtain the zero-mode wave functions, by taking $q=0$, $E=0$; we recover the amplitudes $(a_{+1},a_{-1})=(i-\tau,\tau+i)$. The complete wave functions of the zero modes are

$$\psi^0_{\sigma\tau} = \chi_\sigma \otimes \chi_\tau \otimes e^{-x(\Delta/v)}[i(1+i\tau)\psi_0 e^{+i(\mu/v)x} - i(1-i\tau)\eta^z\psi_0^* e^{-i(\mu/v)x}], \tag{60}$$

where $\psi_0=(\sigma\tau,-\sigma\tau,1,1)^T$. We find a total of four zero modes $(\sigma,\tau=\pm 1)$.

The particle-hole relation of the BCS Hamiltonians that—given an eigenstate ψ_E with energy E, $\omega^x\psi_E^*$ is also an eigenstate with energy $-E$, when applied to the four zero modes we find here—gives four states that are *orthogonal* to the zero modes we found. This surprising result is understood when considering how the boundary condition behaves. Starting from $\omega^z\eta^y\tau^y\psi=\psi$, we want to know what boundary condition is satisfied by $\bar{\psi}=\omega^x\psi^*$. It can be easily shown that the boundary condition is $\omega^z\eta^y\tau^y\bar{\psi}=-\bar{\psi}$. This result shows us that the $\bar{\psi}$ states are *precisely* the ones discarded by the boundary condition in this case. Therefore, the only states satisfying the boundary conditions are the four zero modes we have found above. Finally, it is amusing to mention another consequence of these boundary conditions—the superposition yielding a Majorana fermion $\psi+\bar{\psi}$—*cannot* be taken here. Therefore, despite the existence of zero modes, they cannot form Majorana fermion states.

The edge states energy spectrum at low momentum q is linear in the momentum, and we now proceed to briefly calculate the approximate edge state wave functions for these low energies. The boundary conditions, cast as linear equations in the coefficients a_η, can be linearized in energy and momentum. In this case the energy quantization condition we derive is

$$E = \frac{\Delta q\tau v(qv+2\Delta)}{\Delta(qv+2\Delta)+2\mu^2-qv\mu\tau}, \tag{61}$$

with $\omega=\pm 1$. Linearizing in momentum q, this result reduces to Eq. (59). The solution for a_η we find with this value of E is $a_{+1}=a_{-1}^*=(\Delta-i\mu)[qv+(\Delta+i\mu)(i\tau+1)]$. With these coefficients, linearizing everything in momentum q yields

$$\psi_{\sigma,\tau} = \chi_\sigma \otimes \chi_\tau \otimes e^{-x(\Delta/v)+iqy}[e^{+i(\mu/v)x}\Psi a_{+1} + e^{-i(\mu/v)x}\eta^z\Psi^* a_{+1}^*], \tag{62}$$

where

$$\Psi = \begin{pmatrix} (\Delta^2+i(\Delta+iE)(E-\mu))\sigma\tau \\ -(\Delta+iE)(qv+\Delta-i\mu)\sigma\tau \\ \Delta(qv+\Delta-i\mu) \\ \Delta(\Delta-i\mu) \end{pmatrix}. \tag{63}$$

We find that every energy level has a fourfold degeneracy, including the zero modes. This is the minimal expected degeneracy, required by the SU(2) symmetries of both the spin and the valley spinor. Since the zero modes posses only this minimal degeneracy as well, it is topologically protected.

Considering the quadratic correction to the kinetic-energy term since the zero modes only vary in the x direction, the splitting term reduces to Eq. (39). A straightforward calculation then shows that all the matrix elements between the zero-mode wave functions $\psi^0_{\sigma\tau}$ vanish, and we find that there is no splitting to first order. This is in agreement with Sec. VI A because the armchair edge corresponds to the angle $\alpha=0$ in Eq. (43), yielding no splitting.

C. Singlet $p+ip$ condensate

In this subsection, we turn to explore the edge states in the honeycomb spin-singlet condensate p_x+ip_y phase. Starting from the BdG equations Eq. (44), we proceed with a calculation that is only slightly different than that performed for the s-wave phase in Sec. VI B.

The system is translationally invariant in the y direction so we choose solutions of the form $\psi(x,y)=e^{iqy}\psi(x)$. Furthermore, we choose the order-parameter phase $\phi=0$, and solutions that are eigenstates of $\sigma^y\psi=\sigma\psi$ and $\tau^y\psi=\tau\psi$. All this yields

$$[\mu\omega^z - iv\hat{D} - \Delta\omega^x\eta^y\hat{D}\tau\sigma]\psi = E\psi, \tag{64}$$

where $\hat{D}=(\eta^x\partial_x+\omega^z\eta^y iq)$. Boundary condition (54) then requires $\omega^z\eta^y\psi(x=0)=\tau\psi(x=0)$.

We find the solutions to this set of coupled ODEs in the same manner as in Sec. VI B. We find those solutions that are exponentially decaying in $x>0$, and linearize them in momentum and energy, expecting a low-energy relation $E\sim q$. We find the general (linearized) solution

$$\psi_{\eta\sigma\tau} = \chi_\sigma \otimes \chi_\tau \otimes e^{ix\eta\mu/v - i\Delta\eta} \times \begin{Bmatrix} i[ivE+\Delta\eta(E+\mu)]\sigma\tau \\ [vE\eta+q\Delta(v-i\Delta\eta)\eta-i\Delta(E+\mu)]\sigma\tau \\ \Delta\eta[q(\Delta+iv\eta)+\mu] \\ \Delta\mu \end{Bmatrix}, \tag{65}$$

where $\eta=\pm 1$. We take the general solution $\psi=\Sigma_\eta\psi_\eta a_\eta$ and find which coefficients a_η will satisfy the armchair boundary conditions. The set of equations for a_η can be cast in a matrix form, and for a nontrivial solution to exist, the matrix determinant must vanish. This yields the approximate quantization condition for the low-energy spectrum

$$2\Delta\sigma\{\Delta(v^2+\Delta^2)q^2+[Ev^2+\Delta^2(E+2\mu)]q-2vE\mu\tau\}=0, \tag{66}$$

with the solutions

$$E=-\frac{\Delta(q^2v^2+q^2\Delta^2+2q\Delta\mu)}{qv^2-2\mu\tau v+q\Delta^2}\approx\frac{\Delta^2\tau q}{v}+O(q^2). \tag{67}$$

As expected, we indeed find a branch of low-energy states with energy linear in the transverse momentum, and zero modes for $q=0$. Next, we find the approximate edge state wave functions. The solutions for the coefficients are

$$a_\eta = q(\Delta-\eta iv)+\mu+i\mu\eta\tau. \tag{68}$$

The full edge state wave functions we find then, after linearizing them with respect to the momentum q, are

$$\psi_{\sigma\tau} = \chi_\sigma\otimes\chi_\tau\otimes e^{-x\Delta\mu/v^2+\Delta^2+iqy} \times\left[\cos\left(\frac{vx\mu}{v^2+\Delta^2}\right)\begin{pmatrix}\sigma(q(\tau v^2-\Delta v-\Delta^2\tau)-v\mu)\\ i\sigma(q(v^2-\Delta\tau v-\Delta^2)-v\mu\tau)\\ iv(q\Delta+\mu)\tau\\ v(q\Delta+\mu)\end{pmatrix} + \sin\left(\frac{vx\mu}{v^2+\Delta^2}\right)\begin{pmatrix}-\sigma(q\Delta^2+v\mu\tau)\\ i\sigma(v\mu+q\Delta(2v+\Delta\tau))\\ -iv(-2q\Delta-\mu+qv\tau)\\ v(qv-\mu\tau)\end{pmatrix}\right]. \tag{69}$$

We find every low-energy state is fourfold degenerate—for $E\neq 0$, there is spin degeneracy, and a twofold degeneracy of the product τq. For the zero modes ($q=0$) there is still a fourfold degeneracy, in both spin and valley spinor degeneracy. As for the *s*-wave case, this is the minimal degeneracy of each energy level, and as such, the zero modes are topologically protected.

Finally, we turn to examine what influence the quadratic correction to the kinetic energy has over the zero modes, since this perturbation breaks the valley spinor SU(2) symmetry. As in the *s*-wave case, the zero modes have no y dependence, so the correction reduces to Eq. (39). A straightforward calculation of the matrix elements between the different zero modes yields these all vanish, and so there is no splitting from this correction, to first order.

VII. VORTEX-CORE ZERO-MODE BOUND STATES

In this section we will investigate whether zero-mode bound states at vortex cores exist, in various phases.

A. Singlet *s*-wave condensate

The simple *s*-wave singlet-pairing condensate phase on the honeycomb lattice has an eigenvalue spectrum determined by the BdG equation

$$(\mathcal{H}_0+\mathcal{H}_1)\psi = E\psi, \tag{70}$$

where we refer to Eqs. (21) and (22) for the full details of the kinetic and pairing term. In this section we will find the zero-mode solutions in Eq. (70) explicitly. As opposed to the calculation of Ref. 19, we allow for a nonzero chemical potential (corresponding to slight deviations from half filling), and we find *exact* solutions for the zero modes.

As a first step, we choose solutions that are $\sigma^y\tau^y$ eigenstates, precisely as in the SNS and edge geometries, and as a result the energy spectrum will be at least fourfold degenerate. We will model the vortex by assuming the form $-i\Delta_0=\Delta(r)e^{i\phi}$, with $\Delta(r)$ real.

We begin by considering the half filling case ($\mu=0$). The BdG equation then become

$$\begin{pmatrix}-iv(\vec{\eta}\cdot\nabla) & \Delta(r)e^{i\phi}\eta^y\sigma\tau\\ \Delta(r)e^{-i\phi}\eta^y\sigma\tau & -iv(\vec{\eta}^*\cdot\nabla)\end{pmatrix}\psi=0. \tag{71}$$

In this special case, one can obtain solutions that exist on only one of the two sublattices. This becomes obvious when multiplying the equation set $\mathcal{H}\psi=0$ by η^y on the left, resulting in

$$\begin{pmatrix}-iv(-i\eta^z\partial_x+\partial_y) & \Delta(r)e^{i\phi}\sigma\tau\\ \Delta(r)e^{-i\phi}\sigma\tau & -iv(-i\eta^z\partial_x-\partial_y)\end{pmatrix}\psi=0. \tag{72}$$

We can then choose to consider a solution on one of the sublattices 1,2 in which case $\eta^z\to\eta=\pm 1$. Writing the equations in polar coordinates

$$\begin{pmatrix}-v\eta e^{+i\eta\phi}\left(\partial_r+\frac{i\eta}{r}\partial_\phi\right) & \Delta(r)e^{+i\phi}\sigma\tau\\ \Delta(r)e^{-i\phi}\sigma\tau & -v\eta e^{-i\eta\phi}\left(\partial_r-\frac{i\eta}{r}\partial_\phi\right)\end{pmatrix}\psi=0. \tag{73}$$

We observe that a for $\eta=+1$, we can try a solution $\psi=(u,v)$, where u,v are independent of the angle ϕ, and for $\eta=-1$, we can try a solution of the form $\psi=\frac{1}{r}(e^{i\phi}u,e^{-i\phi}v)$. For both choices, the equations reduce to

$$\begin{pmatrix} -v\partial_r & \Delta(r)\eta\sigma\tau \\ \Delta(r)\eta\sigma\tau & -v\partial_r \end{pmatrix}\begin{pmatrix} u \\ v \end{pmatrix} = 0. \quad (74)$$

Rewriting these equations using the Nambu Pauli matrices

$$[-v\partial_r + \Delta(r)\eta\sigma\tau\omega^x](u,v)^T = 0, \quad (75)$$

it becomes clear the solutions are ω^x eigenstates,

$$\begin{pmatrix} u \\ v \end{pmatrix} = \begin{pmatrix} 1 \\ \omega \end{pmatrix}\exp\left[\eta\sigma\tau\omega\frac{1}{v}\int_0^r dr'\Delta(r')\right]. \quad (76)$$

Already at this point, before taking into account normalizability, we see that as many as 16 zero-mode solution exist, parametrized by $\eta,\sigma,\tau,\omega=\pm 1$. Assuming that $\Delta(r)$ is positive at $r\to\infty$, only half of these 16 solutions are exponentially decaying $\eta\sigma\tau\omega=-1$, and thus normalizable in an infinite system. The number of zero modes is then reduced to eight. In a finite system the exponentially growing solutions correspond to edge states.

The full wave-function solutions we find are, for $\eta=+1$,

$$\psi_1 = \chi_\tau \otimes \chi_\sigma \otimes \begin{pmatrix} 1 \\ 0 \\ \omega \\ 0 \end{pmatrix}\exp\left[+\sigma\tau\omega\frac{1}{v}\int_0^r dr'\Delta(r')\right], \quad (77)$$

and for $\eta=-1$

$$\psi_2 = \chi_\tau \otimes \chi_\sigma \otimes \frac{1}{r}\begin{pmatrix} 0 \\ e^{i\phi} \\ 0 \\ \omega e^{-i\phi} \end{pmatrix}\exp\left[-\sigma\tau\omega\frac{1}{v}\int_0^r dr'\Delta(r')\right]. \quad (78)$$

Here, as in Sec. VI C, the four-component vectors correspond to $(u_1,u_2,v_1,v_2)^T$ (1 and 2 are the sublattice indices). We will follow this convention in the remainder of this section. With the condition of normalizability, the exponentials must take on the decaying form $\exp[-\frac{1}{v}\int_0^r dr'\Delta(r')]$, and we must have $\omega=-\sigma\tau\eta$. The solutions then become

$$\psi_{1,2} = \chi_\tau \otimes \chi_\sigma \otimes \psi_{1,2}^0 \exp\left[-\frac{1}{v}\int_0^r dr'\Delta(r')\right], \quad (79)$$

where $\psi_1^0=(1,0,\sigma\tau,0)^T$ and $\psi_2^0=\frac{1}{r}(0,e^{i\phi},0,\sigma\tau e^{-i\phi})^T$.

Next we turn to normalizability in the $r\to 0$ limit. This is determined by whether the integral $\int_0^{r_0}|\psi|^2 r dr$ diverges. The solution ψ_1 is clearly normalizable in this region, while ψ_2 clearly is not. This leaves us with four zero modes, rather than eight as we found for the SNS junction, where no analog of the $r\to 0$ normalizability condition appears.

Now we turn to the case away from half filling. The BdG equations in this case read

$$\begin{pmatrix} \mu - iv(\vec{\eta}\cdot\nabla) & \Delta(r)e^{i\phi}\eta^y\sigma\tau \\ \Delta(r)e^{-i\phi}\sigma\tau & -\mu - iv(\vec{\eta}^*\cdot\nabla) \end{pmatrix}\psi = 0. \quad (80)$$

We can eliminate the ϕ dependence from the problem by choosing the exact same form as in the half-filling case

$$\psi(r,\phi) = [u_1(r), e^{i\phi}u_2(r), v_1(r), e^{-i\phi}v_2(r)]^T. \quad (81)$$

The reduced ODEs (ordinary differential equations) then involve only the radial coordinate.

At this point it is useful, to make the educated guess

$$\psi(r,\phi) = \begin{pmatrix} u_1(r) \\ e^{i\phi}u_2(r) \\ v_1(r) \\ e^{-i\phi}v_2(r) \end{pmatrix}\exp\left[-\frac{1}{v}\int_0^r dr'\Delta(r')\right], \quad (82)$$

inspired by the form of the solution for the SNS junction. Plugging this form into the ODEs, does not remove the order parameter from them completely. However, choosing $v_1(r)=-\sigma\tau u_1(r)$ and $v_2(r)=\sigma\tau u_2(r)$ in addition does remove the order parameter. The reduced ODEs, involving only $u_{1,2}$, then read

$$\mu u_2(r) - iv u_1'(r) = 0,$$

$$\mu u_1(r) - \frac{iv u_2(r)}{r} - iv u_2'(r) = 0. \quad (83)$$

Extracting u_2 from first equation, and plugging it into the second yields a single ODE for u_1,

$$\frac{u_1'(r)v^2}{r\mu} + \frac{u_1''(r)v^2}{\mu} + \mu u_1(r) = 0. \quad (84)$$

The solutions are Bessel functions $J_0(\frac{r\mu}{v})$, $Y_0(\frac{r\mu}{v})$, and u_2 is obtained from $u_2(r)=\frac{iv u_1'(r)}{\mu}$. The two zero-mode solutions we obtain are then

$$\psi = \chi_\tau \otimes \chi_\sigma \otimes \exp\left[-\frac{1}{v}\int_0^r dr'\Delta(r')\right]\begin{pmatrix} J_0\left(\frac{r\mu}{v}\right) \\ -ie^{i\phi}J_1\left(\frac{r\mu}{v}\right) \\ -\sigma\tau J_0\left(\frac{r\mu}{v}\right) \\ -ie^{-i\phi}\sigma\tau J_1\left(\frac{r\mu}{v}\right) \end{pmatrix}, \quad (85)$$

and the second solution simply has all the Bessel functions of the first kind replaced with Bessel functions of the second kind, with the same parameters. Only the Bessel functions of the first kind is normalizable in $r\to 0$, or alternatively [specifically $\int_0^{r_0}Y_1(\frac{r\mu}{v})^2 r dr$ diverges], if we impose a boundary condition at some small $r=a$, we will pick out some combination of the two Bessel function kinds. With the σ,τ degeneracy we end up with four zero modes. It is easy to verify that the BCS particle-hole relation yields $\omega^x(\psi_{1,2}^{\sigma\tau})^*=-\sigma\tau\psi_{1,2}^{-\sigma,-\tau}$ producing no new zero modes beyond the four mandated by the system symmetries.

It is noteworthy that the Bessel function, far from the vortex core $\frac{r\mu}{v}\gg 1$, has an oscillatory nature, with a length scale $\frac{v}{\mu}$, precisely as in the zero modes we find for the SNS and edge states.

B. Singlet $p+ip$ condensate

We turn now to the simple p_x+ip_y singlet-pairing condensate phase. The vortex-core eigenvalue spectrum is determined by the BdG equation

$$(\mathcal{H}_0 + \mathcal{H}_2)\psi = E\psi, \tag{86}$$

where Eqs. (21) and (23) contain the full details of the kinetic and pairing term.

As in the s-wave case, we choose solutions that are $\sigma^y\tau^y$ eigenstates, precisely as in the SNS and edge geometries, and as a result the energy spectrum will be at least fourfold degenerate. We will model the vortex by assuming the form $i\Delta_1 = \Delta(r)e^{+i\phi}$, with $\Delta(r)$ real (different from our conventions in earlier sections so that we can use the same ansatz for the polar angle dependence as for the s-wave case). Also, since it will prove convenient, we will assume that the order-parameter radial profile is piecewise uniform—vanishing inside the vortex core, and constant outside it.

With the insight gained in the previous subsection, we find the ϕ dependence can be eliminated from the zero-mode problem by choosing the wave-function form

$$\psi(r,\phi) = [u_1(r), e^{i\phi}u_2(r), v_1(r), e^{-i\phi}v_2(r)]^T. \tag{87}$$

The reduced ODEs then involve only the radial coordinate, and can be cast in the form $\partial_r\psi = A\psi$, where

$$A = -\frac{1}{2r} - \frac{1}{v^2+\Delta^2}\Bigg[\Delta\mu\sigma\tau\omega^y\eta^z + iv\mu\eta^x\omega^z + \frac{\Delta}{2r}v\sigma\tau\omega^x\eta^x - \eta^z\frac{v^2}{2r}\Bigg]. \tag{88}$$

We first find the asymptotic ($r\to\infty$) solutions to the ODE system. Neglecting all the $\frac{1}{r}$ terms, we find

$$A = -\frac{1}{v^2+\Delta^2}[\Delta\mu\sigma\tau\omega^y\eta^z + iv\mu\eta^x\omega^z]. \tag{89}$$

We can diagonalize the asymptotic form of A with the unitary transformation

$$O = \frac{1}{2}\begin{pmatrix} i & -i & -i & i \\ i & i & -i & -i \\ -1 & 1 & -1 & 1 \\ 1 & 1 & 1 & 1 \end{pmatrix}, \tag{90}$$

yielding

$$O^\dagger AO = \frac{\mu}{v^2+\Delta^2}$$

$$\text{Diagonal}(-iv-\Delta\sigma\tau, +iv-\Delta\sigma\tau, -iv+\Delta\sigma\tau, +iv+\Delta\sigma\tau). \tag{91}$$

Using this unitary transformation on the full matrix A, we find a block-diagonal form

$$O^\dagger AO = \begin{pmatrix} \mathcal{A}_{\sigma\tau} & 0 \\ 0 & \mathcal{A}_{-\sigma\tau} \end{pmatrix}, \tag{92}$$

where

$$\mathcal{A}_{\sigma\tau} = -\frac{1}{2r} + \frac{1}{\Delta^2+v^2}\Bigg[-\Delta\mu\sigma\tau + \begin{pmatrix} -iv\mu & \frac{iv\Delta\sigma\tau}{2r} - \frac{v^2}{2r} \\ -\frac{v^2}{2r} - \frac{i\Delta\sigma\tau v}{2r} & iv\mu \end{pmatrix}\Bigg]. \tag{93}$$

Here the terms outside the matrix are implicitly multiplied by 2 by 2 identity matrices.

We now turn to solve the reduced ODE system $\mathcal{A}_{\sigma\tau}\xi = \partial_r\xi$, where $\xi = [f_1(r), f_2(r)]^T$. The precise solution will prove cumbersome to work with, and so we will start with an approximate solution that will reveal all the features of the solutions we need to find. First we write $\xi = \frac{1}{\sqrt{r}}e^{-(\Delta\mu\sigma\tau/\Delta^2+v^2)r}\zeta$. We note at this point that for the solution to be normalizable at $r\to\infty$, we must have $\mu\sigma\tau > 0$, if however this is not the case, then we simply choose the solution for the $\mathcal{A}_{-\sigma\tau}$ sector, in $O^\dagger AO$. The ODE for ζ is then

$$\partial_r\zeta = \frac{1}{\Delta^2+v^2}\begin{pmatrix} -iv\mu & \frac{iv\Delta\sigma\tau}{2r} - \frac{v^2}{2r} \\ -\frac{v^2}{2r} - \frac{i\Delta\sigma\tau v}{2r} & iv\mu \end{pmatrix}\zeta. \tag{94}$$

Now we assume that $v \gg \Delta$, and consider the small r limit, so that we can approximate

$$\partial_r\zeta \approx -\frac{1}{2r}\begin{pmatrix} 0 & 1 \\ 1 & 0 \end{pmatrix}\zeta, \tag{95}$$

for which the solutions are

$$\zeta_\eta = (1,\eta)^T r^{-\eta/2}. \tag{96}$$

In the limit $r\to 0$, only the $\eta = +1$ solution is normalizable. We, therefore, find approximate solutions that have only the σ,τ fourfold degeneracy.

We now turn to briefly make connection with the precise solutions for the zero modes. From the equation $\partial_r f_1 = \ldots$, we extract $f_2(r)$, and substitute it in the other equation. This yields a single second-order ODE

$$[\Delta^2 + 8r\mu\sigma\tau\Delta + 4r\mu(iv + r\mu)]f_1(r) + 8r(v^2+\Delta^2 + r\Delta\mu\sigma\tau)f_1'(r) + 4r^2(v^2+\Delta^2)f_1''(r) = 0. \tag{97}$$

Next, we write $f_1(r) = g(r)e^{-r\mu(iv+\Delta\sigma\tau)/v^2+\Delta^2}r^{1/2(v/\sqrt{v^2+\Delta^2}-1)}$, and furthermore replace the radial variable with $r = -\frac{iz(v^2+\Delta^2)}{2v\mu}$. The ODE for $g(r)$ is then

$$-\frac{vg(z)}{2\sqrt{v^2+\Delta^2}} + \left(\frac{v}{\sqrt{v^2+\Delta^2}} - z + 1\right)g'(z) + zg''(z) = 0, \tag{98}$$

which is the confluent hypergeometric ODE. The solutions are

$$g(z) = c_1 M(a, 1+2a, z) + c_2 z^{-2a} M(-a, 1-2a, z), \tag{99}$$

where $c_{1,2}$ are free coefficients, $a = \frac{v}{2\sqrt{v^2+\Delta^2}} \le \frac{1}{2}$ (and also $a > 0$), and $M(a,b,z) = {}_1F_1(a,b,z)$ is the confluent hypergeometric function of the first kind (or Kummer function). With the complex-valued variable $z \sim ir$, the solutions are well behaved at $r\to\infty$. At small r, to lowest order $M(a,b,z) \approx 1 + O(z)$, and the radial part of the wave function behaves

like $f_1(r) \sim r^{-1/2} r^a g(z) \sim r^{-1/2} r^a (c_1 + c_2 r^{-2a} + \ldots) \sim c_1 r^{a-1/2} + c_2 r^{-a-1/2} \sim c_2 r^{-a-1/2}$. When $a < \frac{1}{2}$ this solution is normalizable. However, in the $r \to 0$ limit the order parameter must vanish, so we must take $\Delta = 0$, in which case $a = 1/2$, and causes a logarithmic divergence when we try to normalize it. Therefore, including the $r \to 0$ point, we must set $c_2 = 0$, and we are indeed left with only four solutions for zero modes.

C. Quadratic correction for the vortex-core zero modes

In both cases of the s-wave and $p_x + ip_y$ spin-singlet phases, the eigenstates are angular-momentum eigenstates as well, and have the general separable wave-function form

$$\psi_\ell(r,\phi) = \chi_\sigma \otimes \chi_\tau \otimes e^{i\ell\phi} \begin{pmatrix} u_1(r) \\ e^{i\phi} u_2(r) \\ v_1(r) \\ e^{-i\phi} v_2(r) \end{pmatrix}. \quad (100)$$

We take quadratic correction (25) in polar coordinates and find that it takes this wave function into the form

$$\mathcal{H}_4 \psi_\ell(r,\phi) = \chi_\sigma \otimes \chi_{-\tau} \otimes e^{i\ell\phi} \begin{pmatrix} e^{3i\phi} f_1(r) \\ e^{-2i\phi} f_2(r) \\ e^{-3i\phi} g_1(r) \\ e^{2i\phi} g_2(r) \end{pmatrix}. \quad (101)$$

Then trying to take the product $\langle \psi_{\ell'} | \mathcal{H}_4 | \psi_\ell \rangle$, it suffices to consider the angular dependency

$$\begin{aligned} \langle \psi_{\ell'} | \mathcal{H}_4 | \psi_\ell \rangle \sim & \int_0^{2\pi} d\phi e^{i(\ell'-\ell)\phi} (u_1^*, e^{-i\phi} u_2^*, v_1^*, e^{+i\phi} v_2^*) \\ & \times \begin{pmatrix} e^{3i\phi} f_1(r) \\ e^{-2i\phi} f_2(r) \\ e^{-3i\phi} g_1(r) \\ e^{2i\phi} g_2(r) \end{pmatrix} \\ & \sim \int_0^{2\pi} d\phi e^{i(\ell'-\ell)\phi} [u_1^* f_1 e^{3i\phi} + u_2^* f_2 e^{-3i\phi} \\ & + v_1^* g_1 e^{-3i\phi} + v_2^* g_2 e^{3i\phi}]. \end{aligned} \quad (102)$$

from the polar phase integration we conclude that nonzero matrix elements exist only between states with angular momentum ℓ differing by ± 3. In particular, to first order, there is no correction, and the zero modes persist to this order.

To conclude this section, we point out that the pure Dirac theory approximating the honeycomb lattice allows for topological zero modes to appear bound to vortices in both spin-full condensate phases.

VIII. NUMERICS ON THE HONEYCOMB LATTICE MODEL

In Secs. VII A–VII C we found zero modes exist in both the s-wave and $p_x + ip_y$ spin-singlet states in the continuum Dirac approximation for the honeycomb lattice. We also tried to ascertain whether the zero modes exist beyond the approximate Dirac theory for the honeycomb lattice, by taking into account the quadratic correction to the kinetic energy Eq. (25). We calculated whether this correction splits the zero modes at first order in perturbation theory. With the exception of one case, we always found that to first order, no splitting occurs. The exception is the s-wave phase in the SNS geometry with $\alpha \neq 0$ (Sec. V A), where we found the correction *does* give a splitting to first order in the quadratic correction. In contrast, in the edge state and vortex cases, no such splitting occurred at first order. While the SNS splitting does vanish when the junction boundaries are of the armchair edge type, consistent with the edge state result, the collection of these results is inconclusive as to whether the zero modes really do appear in the lattice model, and not just in the idealized approximate Dirac theory. To answer this question definitively, we have performed numerical calculations (exact diagonalization) on the precise lattice models for all phases where we suspect zero modes occur.

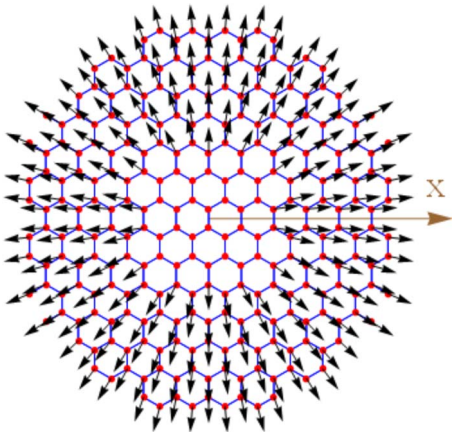

FIG. 7. (Color online) Circular lattice patch in the vortex state. The (black) arrows represent the phase at a lattice point as the angle the arrow makes with the x axis in the picture. The (red) dots are the honeycomb lattice sites, and (blue) lines are the nearest-neighbor links. Here, for illustration purposes, the radius of the vortex core is taken to be 2 (the radius of the lattice patch is 6, where the nearest-neighbor distance is $1/\sqrt{3}$). Following the arrows it can be verified that the vortex indeed has a unit vorticity.

We consider the vortex state case of the two spin-singlet phases at precisely half filling. First, we constructed lattice patches of square, rectangular, circular, and elliptic shapes (see Fig. 10 for illustrations), of various sizes. We then diagonalized the matrices describing lattice model (6) on these lattice patches, with the two spin-singlet order parameters including unit-vorticity vortices at their centers (one representative example is shown in Fig. 7). In all cases, we find the lowest-energy eigenvalues E_0, and compare them with the de Gennes energy scale $\frac{E_g^2}{E_F}$, the energy scale one expects for vortex-core bound state.[20] For the s-wave state, the gap energy $E_g = \Delta$, while for the spin-singlet $p_x + ip_y$ state, the gap scales with chemical potential (21) $E_g \sim \mu$. The sizes of the various lattice patch geometries we take is detailed in Table II, where the nearest-neighbor distance is $1/\sqrt{3}$ (the primitive Bravais lattice vectors are then of length 1). The scaling of the lowest energy with the finite system size is described in

TABLE II. Lattice patch sizes.

Square		Circular		Rectangular		Elliptic	
L	Sites	L	Sites	L	Sites	L	Sites
12	350	8	466	6	137	3	130
14	464	9	590	8	238	4	222
16	611	10	726	10	357	5	358
18	777	11	874	12	525	6	512
20	943	12	1036	14	696	7	700
22	1147	13	1226	16	924	8	922
24	1372	14	1416	18	1147	9	1162
26	1590	15	1630	20	1415	10	1446
28	1824	16	1858	22	1710	11	1746

Fig. 8 for the s-wave state, and in Fig. 9 for the spin-singlet p_x+ip_y state. It is clear from all scaling plots that the lowest energy is of order of the de Gennes energy, and that this energy does not significantly decrease with growing system size. This would indicate that there exist no zero modes in these phases, despite the results from the continuum Dirac theory.

In addition, we plot the spatial density of the lowest-energy quasiparticle density on the lattice patch, in a number of representative cases in Figs. 10 and 11, in order to verify that these indeed are vortex-core bound states. Specifically, at each lattice site j we plot a dot with its color signifying the relative magnitude of $|u_j|^2+|v_j|^2$ (the values are normalized to run between 0 and 1, and the color is varied linearly with this value). From the plots it is clear that these lowest-energy states are indeed vortex-core bound states.

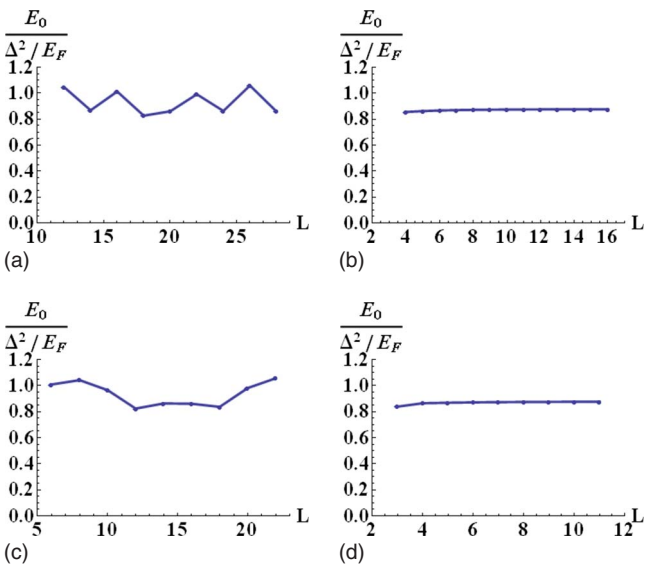

FIG. 8. (Color online) Scaling of the lowest energy with lattice patch size. We plot the ratio of the lowest energy to the de Gennes energy for all sizes we take. The square lattice patch (a) is of size $L\times L$, the circular lattice patch (b) is of radius L, the rectangular lattice patch (c) is of dimensions $L\times\frac{3}{2}L$, and the elliptic lattice patch (d) is of main axis' L and $2L$. The corresponding number of sites for each lattice patch is detailed in Table II. It is clear from the graphs that the lowest energy is always of the order of the de Gennes energy, and remains roughly unchanged when we increase the system size.

In all the cases described in Figs. 8 and 9, the vortex-core size was taken to be 0, forcing the vortex phase winding to occur over a distance that is comparable to the lattice length scale. This fact is what invalidates the Dirac continuum theory—the order parameter in these cases is *not* a slowly varying function on the lattice scale, near the vortex core. Following this last observation, we also calculated the energy spectrum for a series of different vortex-core sizes, ranging from 0.2 to 5.8 in increments of 0.4, while keeping fixed the overall system size (circular lattice patch of radius 12.0). The results are plotted in Fig. 12 and it is clear from them that the energy splitting decreases rapidly with the vortex-core size. The highest energy we find (at the smallest radius) is 0.88 times the de Gennes scale, and the smallest energy scale we find is 0.0016 (at a radius of 5.0). However, the de Gennes energy scale in terms of the correlation length of a superconductor is actually $\frac{\Delta}{k_F\xi}$.[20] From this we expect that the lowest energy should change with the vortex-core

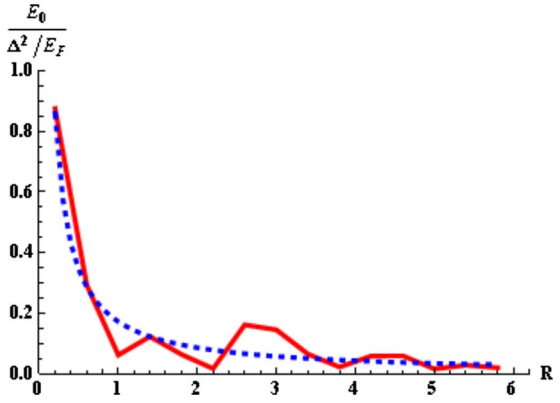

FIG. 9. (Color online) Ratio of lowest-energy scale to de Gennes energy scale, with varying vortex-core size. The vortex-core sizes range from 0.2 to 6.0 in increments of 0.4, and the lattice patch is circular with a radius of 6.0. The nearest-neighbor distance is $1/\sqrt{3}$. The raw data is denoted by the continuous (red) curve, and the fit is denoted by a dashed (blue) curve.

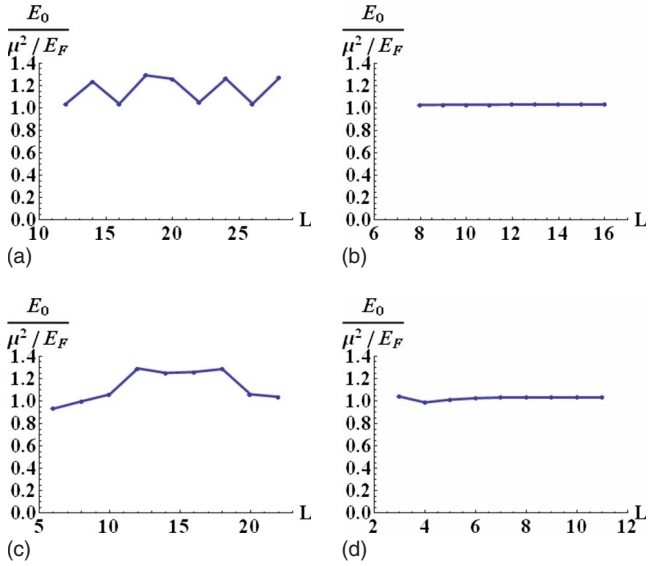

FIG. 10. (Color online) Scaling of the lowest energy with lattice patch size. We plot the ratio of the lowest energy to the de Gennes energy for all sizes we take, for the spin-singlet p_x+ip_y state. In this case, the gap energy scales like the chemical potential μ, so we take as the de Gennes energy scale μ^2/E_F. The square lattice patch (a) is of size $L\times L$, the circular lattice patch (b) is of radius L, the rectangular lattice patch (c) is of dimensions $L\times\frac{3}{2}L$, and the elliptic lattice patch (d) is of main axis' L and $2L$. The corresponding number of sites for each lattice patch is detailed in Table II. It is clear from the graphs that the lowest energy is always of the order of the de Gennes energy, and remains roughly unchanged when we increase the system size.

radius R as $E_0\sim\frac{1}{R}$. We fit the raw data in Fig. 12 to a curve $-0.0007+0.17/R$, also displayed in Fig. 12. When the vortex-core size is bigger, the phase winding occurs over a larger distance, and the approximation of a slowly varying order parameter improves, but the lowest energy is *still* of the de Gennes scale. We find, therefore, that the zero modes are split, and correspond to the de Gennes bound-state spectrum.

For a vortex one would expect the core size to be of the order of the correlation length in the superconducting state. The parameters we use are $\Delta=0.5$, $t=1.0$ the lattice constant $a=1.0$ and working in units where $\hbar=1$, we have a correlation length that is of the order of the lattice constant $\xi\sim\frac{\hbar v_F}{\pi\Delta}\sim\frac{\hbar 3ta}{2\pi\Delta}\sim 1$. In Fig. 12 we can see that for this core size, the lowest energy is between five and ten times smaller than the de Gennes scale.

In conclusion, the numerics we have done show that the zero modes appearing in the continuum Dirac theory are split in the lattice model, but that the bound-state energy can be significantly smaller than the de Gennes scale.

IX. EXPERIMENTAL REALIZATIONS—BOSE FERMI MIXTURES

Superconductivity, which appears in many conventional fermionic systems, does not seem to occur intrinsically in graphene, the most readily available realization of the honeycomb tight-binding model, but can be induced via the proximity effect close to another superconducting material.[32,33] The peculiar band structure of the honeycomb lattice is not however limited to grapheme—it is just one material realization (other possibilities may include thin films of quasi-2D honeycomb layered superconductors[34–36]). Another possibility is a cold fermion gas trapped in an optical lattice, with a fermionic atom density corresponding to about half filling. Since the atoms are electrically neutral, the interactions between them are to a good approximation simple collisions, corresponding to an on-site interaction in a lattice model. Superconductivity requires some attraction between fermions, so in order to have any hope of realizing such a phase, one needs to cause attractive interactions between the fermions. In solids, phonons provide this mechanism by inducing an attractive interaction between electrons. In cold atom gases, this role can be assumed by adding bosonic atoms; sound modes in a Bose-Einstein condensate

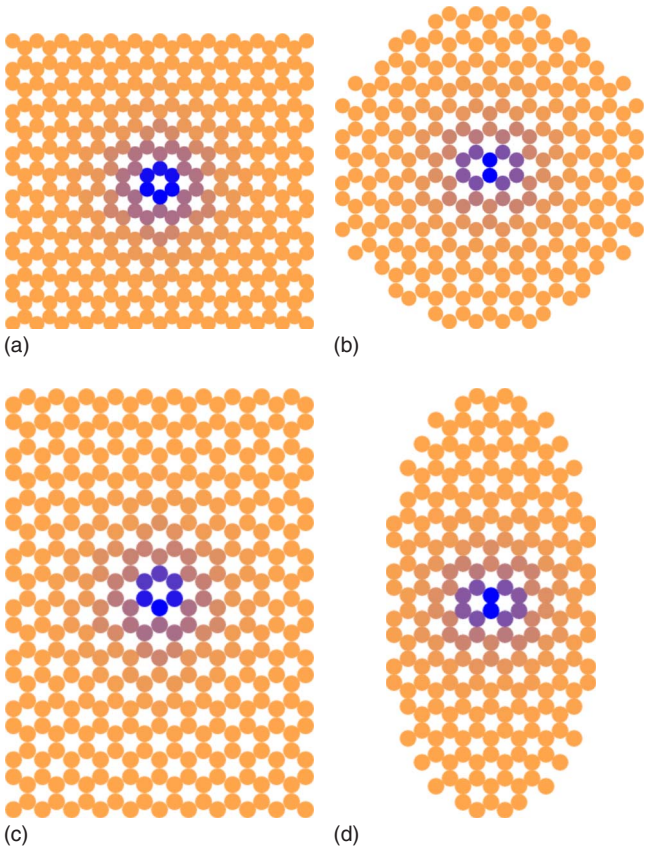

FIG. 11. (Color online) The lowest-energy quasiparticle state wave-function density in the s-wave state, in the (a) square, (b) circular, (c) rectangular, and (d) elliptic geometries. The density $|u_j|^2+|v_j|^2$ at each site j is represented by the color of the dot at each lattice site. The highest density is colored blue (black), and zero density is colored orange (light gray). It is clear in all cases that the lowest-energy state is bound to the vortex core at center of the geometry. Here the vortex-core size was taken to be 0. With the nearest-neighbor distance taken to be $1/\sqrt{3}$, the square (a) lattice patch has dimensions 12×12 (350 sites), the circular (b) lattice patch has radius of 6 (262 sites), the rectangular (c) lattice patch has dimensions 10×15 (357 sites), and the elliptic (d) lattice patch has main axis of length 4 and 8 (222 sites).

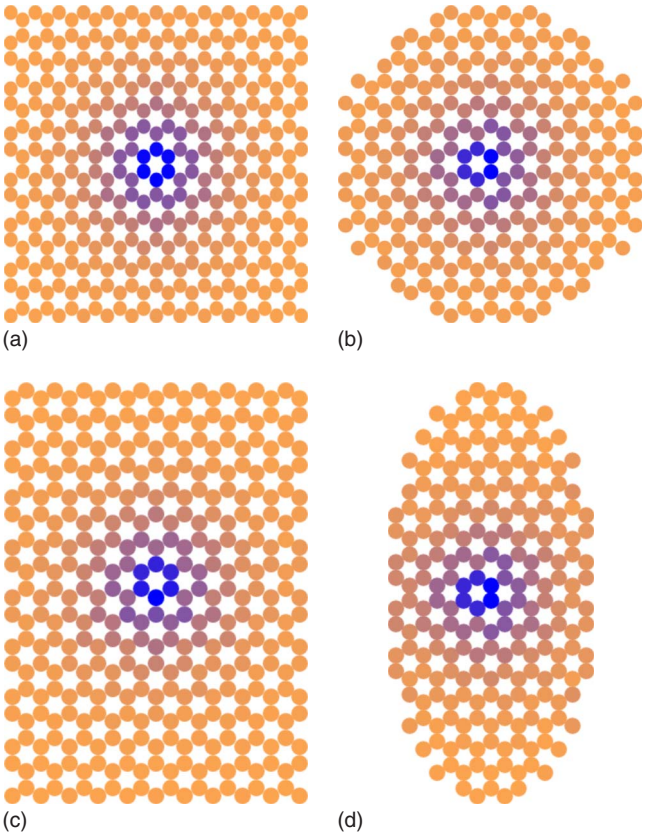

FIG. 12. (Color online) The lowest-energy quasiparticle state wave-function density in the spin-singlet p_x+ip_y state, in the (a) square, (b) circular, (c) rectangular, and (d) elliptic geometries. The density $|u_j|^2+|v_j|^2$ at each site j is represented by the color of the dot at each lattice site. The highest density is colored blue (black), and zero density is colored orange (light gray). It is clear in all cases that the lowest-energy state is bound to the vortex core at center of the geometry. Here the vortex-core size was taken to be 0. With the nearest-neighbor distance taken to be $1/\sqrt{3}$, the square (a) lattice patch has dimensions 12×12 (350 sites), the circular (b) lattice patch has radius of 6 (262 sites), the rectangular (c) lattice patch has dimensions 10×15 (357 sites), and the elliptic (d) lattice patch has main axis of length 4 and 8 (222 sites).

mimic phonons in a solid. The virtues of the cold atom realization do not end in simply making the superconducting state feasible, but also provide a great deal of control over many parameters.

Motivated by the reasoning discussed in the previous paragraph, we will now consider a model of a Bose-Fermi mixture on the honeycomb lattice model. We consider only on-site interactions since usually one has to work quite hard to make longer-range interactions appreciable compared to them in cold atom systems. Our Hamiltonian, therefore, reads

$$\mathcal{H} = -t\sum_{\langle ij\rangle,\alpha} f_{i\alpha}^{\dagger} f_{j\alpha} + \mu\sum_{j,\alpha} f_{j\alpha}^{\dagger} f_{j\alpha} - w\sum_{\langle ij\rangle} b_i^{\dagger} b_j + 3w\sum_j b_j^{\dagger} b_j + U_{bb}\sum_j [(b_j^{\dagger} b_j) - \rho_0]^2 + U_{ff}\sum_j (f_{j\uparrow}^{\dagger} f_{j\uparrow})(f_{j\downarrow}^{\dagger} f_{j\downarrow}) + U_{bf}\sum_j \sum_{\alpha} (f_{j\alpha}^{\dagger} f_{j\alpha})(b_j^{\dagger} b_j), \quad (103)$$

where b_j are bosonic operators and $f_{j,\alpha}$ are the fermionic operators used in our manuscript. As before i,j are used to denote lattice sites, and the two greek letters α,β will be used to denote the spin indices $\uparrow,\downarrow$. The bosonic chemical potential is tuned to the value $3w$—so that the bosonic band minimum is at zero energy, and ρ_0 is the boson density per site.

With no interaction between the boson and fermions, for small $U_{bb}/w \ll 1$ the bosons will condense into a superfluid state. We assume we are deep in such a phase, and that the interactions with the fermions do not destroy the boson superfluidity. We then use standard Bogoliubov theory to approximate the momentum space bose operators $b_\mu(\mathbf{q}) \approx \sqrt{N_0}\delta(\mathbf{q}) + b_\mu(\mathbf{q})$, where the second term is implicitly taken for only nonzero momentum. Here N_0 is half the total number of bosons. The bosonic density operator then becomes $\rho_\mu(\mathbf{q}) \equiv \Sigma_{\mathbf{k}} b_\mu^{\dagger}(\mathbf{k}-\mathbf{q}) b_\mu(\mathbf{k}) \approx N_0\delta(\mathbf{q}) + \sqrt{N_0}[b_\mu^{\dagger}(-\mathbf{q}) + b_\mu(\mathbf{q})]$. Using the Bogoliubov approximation we expand the bosonic terms of Eq. (103) to quadratic order in the operators $b_\mu(\mathbf{q})$. Our goal is then to integrate out the bosonic degrees of freedom (the action is now Gaussian in the bosonic fields), and in this way find the effective Fermionic interactions that are induced.

Taking only those terms in Eq. (103) involving bosonic operators, and performing a Fourier transformation we find

$$\mathcal{H}_b = w\sum_{\mathbf{q},\mu\nu} b_\mu^{\dagger}(\mathbf{q})(3\delta_{\mu\nu} - \Gamma_{\mu\nu}(\mathbf{q}))b_\nu(\mathbf{q}) + U_{bf}/N\sum_{\mathbf{q}}\sum_{\mu} F_\mu(\mathbf{q})\rho_\mu(-\mathbf{q}) + U_{bb}/N\sum_{\mathbf{q}}\sum_{\mu}[\rho_\mu(\mathbf{q}) - N\rho_0\delta(\mathbf{q})][\rho_\mu(-\mathbf{q}) - N\rho_0\delta(\mathbf{q})], \quad (104)$$

where we have introduced the fermionic density operator $F_\mu(\mathbf{q}) = \Sigma_{\mathbf{k},\alpha} f_{\mu\alpha}^{\dagger}(\mathbf{k}-\mathbf{q}) f_{\mu\alpha}(\mathbf{k})$. It is worth mentioning at this point that the boson density per site $\rho_0 = N_0/N$, where N is the number of unit cells of the lattice.

Assuming N_0 is a macroscopic number, we can expand $\mathcal{H}_b$ in powers of N_0. Keeping only the leading terms, we are left with a quadratic form in the bosonic operators. Next we apply a unitary transformation that diagonalizes the hopping term $b_1(\mathbf{q}) = \frac{1}{\sqrt{2}} e^{+i\theta/2}[a_1(\mathbf{q}) + a_2(\mathbf{q})]$ and $b_2(\mathbf{q}) = \frac{1}{\sqrt{2}} e^{-i\theta/2}[a_1(\mathbf{q}) - a_2(\mathbf{q})]$, where $e^{+i\theta} = \gamma(\mathbf{q})/|\gamma(\mathbf{q})|$ (which implicitly depends on $\mathbf{q}$). At this point it is worthwhile mentioning that $\theta(-\mathbf{q}) = -\theta(\mathbf{q})$, which is extremely useful in the detailed steps of our calculation that have been omitted here. After some rewriting of the Hamiltonian, we arrive at the remarkably separable form

$$\mathcal{H}_b \approx \sum_{\mathbf{q}}\sum_{\mu}(g + \epsilon_\mu(\mathbf{q}))a_\mu^{\dagger}(\mathbf{q})a_\mu(\mathbf{q}) + \frac{g}{2}\sum_{\mathbf{q},\mu}[a_\mu(\mathbf{q})a_\mu(-\mathbf{q}) + h.c.] + \frac{U_{bf}\sqrt{N_0}}{N}\sum_{\mathbf{q}}\left[\frac{1}{\sqrt{2}}(F_1^{\dagger}(\mathbf{q})e^{+i\theta/2} + F_2^{\dagger}(\mathbf{q})e^{-i\theta/2})a_1(\mathbf{q}) + \frac{1}{\sqrt{2}}(F_1^{\dagger}(\mathbf{q})e^{+i\theta/2} - F_2^{\dagger}(\mathbf{q})e^{-i\theta/2})a_2(\mathbf{q}) + h.c.\right] + \ldots, \quad (105)$$

where we have introduced the coupling $g=2U_{bb}\rho_0$, and the band dispersions $\epsilon_1=w(3-|\gamma(\mathbf{q})|)$ and $\epsilon_2=w(3+|\gamma(\mathbf{q})|)$. Note that all the momentum summations above formally exclude the $\mathbf{q}=0$ mode. This will hold throughout the remainder of this section, and so it will remain implicit.

Next we employ a Bogoliubov transformation for each of the two bands ($a_{1,2}$) separately. This is accomplished by the transformation $a_\mu(\mathbf{q})=u_\mu(\mathbf{q})B(\mathbf{q})+v_\mu(\mathbf{q})B^\dagger(-\mathbf{q})$ with $u_\mu(\mathbf{q})=\sqrt{\frac{E_\mu(\mathbf{q})+\epsilon_\mu(\mathbf{q})+g}{2E_\mu(\mathbf{q})}}$ and $v_\mu(\mathbf{q})=-\sqrt{\frac{-E_\mu(\mathbf{q})+\epsilon_\mu(\mathbf{q})+g}{2E_\mu(\mathbf{q})}}$, where $E_\mu(\mathbf{q})=\sqrt{\epsilon_\mu(\mathbf{q})(\epsilon_\mu(\mathbf{q})+2g)}$. The new operators $B(\mathbf{q})$ are canonical bosons, and the Hamiltonian takes the form

$$\mathcal{H}_b \approx \sum_{\mathbf{q}}\sum_{\mu} E_\mu B_\mu^\dagger B_\mu + \frac{U_{bf}\sqrt{N_0}}{\sqrt{2}N}\sum_{\mathbf{q}}[(F_1^\dagger e^{+i\theta/2}+F_2^\dagger e^{-i\theta/2})(u_1+v_1)B_1+(F_1^\dagger e^{+i\theta/2}-F_2^\dagger e^{-i\theta/2})(u_2+v_2)B_2+h.c.]+\ldots, \quad (106)$$

where for the sake of brevity, we have omitted explicit mention of the $\mathbf{q}$ dependence of all the operators and functions such as v,u,E.

In order to integrate out the bosonic fields, we must pass to a path-integral formalism, taking into account the imaginary time derivative. Rewriting this term using the bosonic operators (or complex fields) $B_\mu(\mathbf{q})$ we find the action

$$\mathcal{S}=\int_0^{1/T} d\tau \sum_j b_j^\dagger(\tau)\partial_\tau b_j(\tau) - \int_0^{1/T} d\tau \mathcal{H}_b = \int_0^{1/T} d\tau \sum_q \sum_\mu B^\dagger \partial_\tau B - \int_0^{1/T} d\tau \mathcal{H}_b, \quad (107)$$

where for brevity we have written $B\equiv B_\mu(\mathbf{q},\tau)$. Integrating out the bosonic fields, we find

$$S_{\text{eff}}=-\sum_{\mathbf{q},\mu,\omega_n} h_\mu^\dagger(\mathbf{q},\omega_n)h_\mu(\mathbf{q},\omega_n)\frac{1}{E_\mu(\mathbf{q})-i\omega_n}, \quad (108)$$

where

$$h_1^\dagger=\frac{U_{bf}\sqrt{N_0}}{\sqrt{2}N}(F_1^\dagger e^{+i\theta/2}+F_2^\dagger e^{-i\theta/2})(u_1+v_1),$$

$$h_2^\dagger=\frac{U_{bf}\sqrt{N_0}}{\sqrt{2}N}(F_1^\dagger e^{+i\theta/2}-F_2^\dagger e^{-i\theta/2})(u_2+v_2). \quad (109)$$

If we consider only low-frequency effective interactions ($\omega_n\to 0$), then we can return to a Hamiltonian formulation of our problem with

$$\mathcal{H}_{\text{eff}}=-\sum_{\mathbf{q},\mu} h_\mu^\dagger(\mathbf{q})h_\mu(\mathbf{q})\frac{1}{E_\mu(\mathbf{q})}=-\frac{1}{N}\sum_{\mathbf{q},\mu,\nu} F_\mu^\dagger(\mathbf{q})V_{\mu\nu}(\mathbf{q})F_\nu(\mathbf{q}). \quad (110)$$

The interaction vertex we have introduced $V_{\mu\nu}(\mathbf{q})$ has components

$$V_{11}(\mathbf{q})=V_{22}(\mathbf{q})=U_{bf}^2\frac{\rho_0}{2}\left[\frac{(u_1+v_1)^2}{E_1}+\frac{(u_2+v_2)^2}{E_2}\right],$$

$$V_{12}(\mathbf{q})=V_{21}(-\mathbf{q})=V_{21}^*(\mathbf{q})=e^{+i\theta}U_{bf}^2\frac{\rho_0}{2}\left[\frac{(u_1+v_1)^2}{E_1}-\frac{(u_2+v_2)^2}{E_2}\right]. \quad (111)$$

Note that V_{ij} will be invariant under all the symmetries of the honeycomb lattice, including all lattice translations.

Assuming the fermi level passes near the Dirac nodes of the honeycomb band structure (near half filling). The most significant low-energy excitations of the system then involve the fermionic operators with momenta near the Dirac nodes, at $\pm\mathbf{Q}$. The density-fluctuation operator $F_\mu(\mathbf{q})=\Sigma_{k,\alpha}f_{\mu\alpha}^\dagger(\mathbf{k}-\mathbf{q})f_{\mu\alpha}(\mathbf{k})$ will be significant only when $\mathbf{k}=\pm\mathbf{Q}$ and $\mathbf{k}-\mathbf{q}=\pm\mathbf{Q}$. This results in three possible regions for the exchange momentum:

(i) $\mathbf{q}\approx 0$,
(ii) $\mathbf{q}\approx 2\mathbf{Q}=-\mathbf{Q}$,
(iii) $\mathbf{q}\approx -2\mathbf{Q}=\mathbf{Q}$.

Expanding the function $\gamma(\mathbf{q})$ around these three points, and assuming the order of limits $w\gg g\gg wq^2$, we find

$$\mathcal{H}_{\text{eff}}\approx -\frac{U_{bf}^2}{N^2}N_0\sum_{\mathbf{q}\approx\mathbf{0}}\left[\left(\frac{1}{4g}+\frac{1}{12w}\right)(F_1^\dagger F_1+F_2^\dagger F_2)+\left(\frac{1}{4g}-\frac{1}{12w}\right)(F_1^\dagger F_2+F_2^\dagger F_1)\right] - \frac{U_{bf}^2}{N^2}N_0\frac{1}{3w}\sum_{\mathbf{p}\approx\mathbf{0}}(F_1^\dagger F_1+F_2^\dagger F_2)|_{\mathbf{q}=\pm\mathbf{Q}+\mathbf{p}}. \quad (112)$$

The case of noninteracting bosons $g=0$, corresponds to a different limit than above $w\gg wq^2\gg g=0$. The Bogoliubov spectrum becomes the same as the band structure $E\to\epsilon$, the Bogoliubov transformation parameters simplify to $u=1$, $v=0$, and the long-wavelength limit gives

$$V_{11}(\mathbf{q})=V_{12}(\mathbf{q})=U_{bf}^2\frac{2\rho_0}{3w}\frac{1}{q^2}. \quad (113)$$

We find that in this limit the effective interactions are *long range* in real space, and attractive.

The boson interaction strength g controls the range for the effective interaction $\ell\sim 1/g$. Despite us using a weak-interaction limit in the Bogoliubov theory, when assuming $w\gg g$ we end up having the boson interaction coupling g dominating the nature of the effective interaction, with attractive $\mathbf{q}\approx 0$ interactions. The diagonal terms of the interaction vertex correspond to real-space interactions between sites on the same sublattice. This type of interaction includes on-site interactions, which are expected to be the strongest of this kind. In contrast, the off-diagonal (the $F_1^\dagger F_2$ term) terms of the interaction vertex correspond to real-space interactions between sites on *different* sublattices. The shortest-range interactions in this class are nearest-neighbor interactions. Since the off-diagonal and diagonal terms are comparable in magnitude, we expect an attractive effective nearest neighbor of comparable strength to that of the effective on-site interaction.

From the features of the effective interaction vertex, we are lead to believe that the phenomenological model of Ref. 21 may be an appropriate description of this system, which considers fermions on the honeycomb lattice, with only on-site and nearest-neighbor interactions, parametrized by $g_{1,2}$, respectively. For the range of parameters we find in the present work $g_2<0$, and depending on the strength of U_{ff}, the bare on-site repulsion, we can have either positive or negative sign of g_1. Specifically, we can realize $g_1<0$ when $U_{ff} \ll \frac{U_{bf}^2 N_0}{N^2}(\frac{1}{4g}+\frac{1}{12w})$, and $g_1>0$ when $U_{ff} \gg \frac{U_{bf}^2 N_0}{N^2}(\frac{1}{4g}+\frac{1}{12w})$.

Uchoa *et al.*[21] found via a mean-field analysis that the ground state may be a $p+ip$ superconducting state for $g_2<0$ and $g_1<0$ and a mixed s-wave and $p+ip$ superconducting state for $g_2<0$ and $g_1>0$. Therefore it would seem that for strong bare fermion repulsion U_{ff}, one should expect the p_x+ip_y phase.

X. MAGNETIC FIELD SPLITTING

Within the continuum Dirac theory we found zero modes in all the geometries we considered, topological protection occurs modulo symmetry mandated degeneracy (see Sec. III). The fourfold-degenerate zero modes we found in the two spin-singlet phases are protected as a result of the fourfold degeneracy mandated by the SU(2) symmetries of the spin and the Dirac valley spinor. As first pointed out in Ref. 19, a Zeeman field is found to split the spin-degenerate zero modes of the s-wave phase into Zeeman pairs, with a splitting proportional to magnetic field, at first order in perturbation theory. The magnetic field explicitly breaks the SU(2) spin symmetry, and, therefore, the zero modes can now split. In our approach, it is easy to show this is an *exact* result, and that the zero-mode states remain exact eigenstates of the system, albeit with a nonzero energy.

Without a magnetic field the system is isotropic in the spin sector, and so we are free to choose the direction of the magnetic field in spin space. It is convenient to choose the Zeeman field in the y direction. The zero modes we found satisfy $\sigma^y\psi=\sigma\psi$, and so we have precisely $B\sigma^y\psi=B\sigma\psi$ splitting the zero modes. It is important to point out though that while the mathematical spectrum of the BdG Hamiltonian has four zero modes splitting in to two positive and two negative, the physical excitations of the system consists only of the positive-energy states (because of $\omega^x B\sigma^y\omega^x=B\sigma^y$, the BCS Hamiltonian identity $\omega^x\mathcal{H}\omega^x=-\mathcal{H}^*$ still holds), and so there will be a doublet of lowest-energy excitations, with $E=B$.

Unlike a charged fermion superconductor, in a fermionic superfluid there is no need for a magnetic field to create vortices. In any experimental cold atom apparatus, any magnetic field can be made extremely small. Therefore, it would be a great advantage to realize the spin-singlet phases we discuss in this manuscript in a cold atom system, rather than a solid-state system. If the magnetic field is too weak to destroy the fermion pairing, the only important effect of the magnetic field is to introduce a Zeeman field coupling to the spin degrees of freedom, and the spectrum of vortex-core bound states can be manipulated.

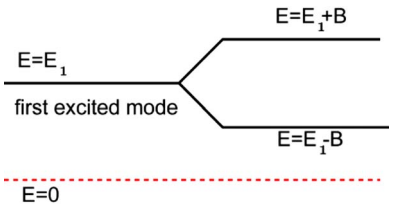

FIG. 13. (Color online) Influence of the Zeeman field splitting on the excitation spectrum in the case that vortex-core zero modes are absent.

Using the Zeeman field splitting of the bound states, we now proceed to propose an experiment to probe whether zero modes exist in these systems (as found in the continuum Dirac theory) or not (expecting the zero modes to split slightly as found in the numerics of Sec. VIII). The magnetic field allows us to control the low-energy spectrum of the system, and this will possibly make it easier to identify in RF (low-frequency) absorption measurements. If we assume all energy states of the experimental system are Kramers doublets, in the absence of zero modes, the lowest-energy excitation (E_1) will be lowered when applying a magnetic field $E=E_1-B$ (see Fig. 13). When zero modes exist, then when applying a magnetic field the lowest excitation energy will move up in energy ($E_0=B$) (see Fig. 14). The lowest excitation energy in the system will then *decrease* with rising magnetic field in the absence of near-zero modes, but will *increase* if they exist in the system. This serves an experimental method to identify the existence of these states, which could easily be carried out in cold atom systems, but are perhaps more difficult in superconducting solid states systems.

XI. DISCUSSION AND CONCLUSION

In this manuscript we have explored whether topological zero modes exist in a number of possible fermionic condensate phases on the honeycomb lattice. We examined two spin-singlet phases both of which are fully gapped in the entire Brillouin zone. We have found that fourfold-degenerate topological zero modes exist within the continuum Dirac theory, for these two phases. We have done this by explicitly solving for zero modes bound to vortex cores,

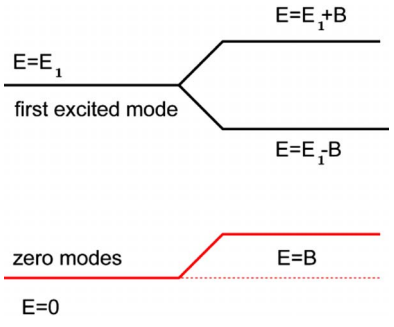

FIG. 14. (Color online) Influence of the Zeeman field splitting on the excitation spectrum in the case that vortex-core zero modes exist.

at sample edges, and in SNS junction geometries. In all cases, the edge state and vortex-core calculations agree completely, with the same degeneracy of zero modes being found, but in the SNS junction geometry an extra accidental symmetry doubles the number of zero modes from four to eight.

With an even degeneracy of vortex-core zero modes, the Majorana zero modes are not compelled to pair into fermionic degrees of freedom between spatially remote vortices, but rather *locally* at each vortex core. The natural mechanism for entanglement of vortex pairs is therefore lost, and no non-Abelian statistics between vortices should appear.

The topological zero modes existence crucially depends on the emergent low-energy SU(2) symmetry of the Dirac valley spinor structure in the Dirac theory. This symmetry does not strictly hold in the original lattice model, and this brings up the possibility that the seemingly protected zero modes found in the Dirac theory are split in the full honeycomb lattice model. While corrections to the Dirac theory give an unclear picture of the fate of the zero modes when the effective low-energy symmetry is broken, the numerical diagonalization we have performed on the lattice model confirm that indeed this is the case—the zero modes are split. In the present context simply using the continuum Dirac model is inaccurate—even when the vortex structure is slowly varying on the scale of the lattice, the Dirac theory is still only approximate, and in fact the zero modes are *not* topologically protected.

We have also discussed the Zeeman field splitting of the vortex-core bound states in this phases. We suggested an experiment taking advantage of this splitting to ascertain whether zero modes exist or not in this system, by tracking how the excitation energies change when modifying the Zeeman field.

In order to realize the experiment we propose, one first needs to create a condensate on the honeycomb lattice. It may be possible to realize a superconducting state in graphene by superconducting leads inducing electron pairing via the proximity effect. Another possibility we have discussed is forming fermion condensates in cold atom Bose-Fermi mixtures. The latter however will most probably require the fermions to be cooled down to very low temperatures compared with the energy scales of optical lattices, which is challenging in current experiments. A cold atom gas is perhaps the ideal realization of the condensate for our proposed experiment since magnetic fields are not involved in the forming of vortices in the first place, and so can be freely manipulated, without affecting the condensate or the vortices too much.

In the context of the zero modes in the "ordinary" p_x+ip_y state, it has already been suggested to probe the bound-state spectrum by RF absorption,[37] and STM (scanning tunneling microscope) measurements.[38] The same tools could be used to probe the bound-state spectrum in the phases we discuss here. As opposed to Refs. 37 and 38, in the experiment we propose one would be looking for how the spectrum moves when changing the magnetic field, rather than simply looking at a static spectrum. It is sometimes more easy to notice something that is moving, rather than stationary, and so it may prove easier to detect the spectrum shifts.

The reaction to magnetic field of the bound states is not limited to vortex cores—it could be discernible in edge states as well if the sample is small enough that the discreteness of the energy levels bound to the edge becomes evident. The edge state spectrum in all the phases we consider here is always linear in the transverse momentum $E \sim qv$, with some effective velocity v. For a finite system, the momentum will be quantized, $q=\frac{\hbar}{2\pi L}(\ell+\gamma)$, and the bound states have a level spacing of $\sim\frac{\hbar v}{2\pi L}$. If the Zeeman splitting as well as the thermal energy scale is smaller than this level spacing, the effect we describe here is in principle observable. In practice, the experimental probe must be sensitive enough to probe these small energy scales.

Finally, our present work has forced us to generalize some ideas that were understood and developed in the context of the ordinary p_x+ip_y state. Topological zero modes were previously understood to be topologically protected only if *single* zero modes existed (in a unit-vorticity vortex). We have generalized this view of topological protection to accommodate symmetry mandated degeneracy of quasiparticle excitations, for which the phases of the continuum Dirac theory we considered are examples. Our conclusion is that zero modes can be protected to all perturbations that preserve the symmetries, and as such are protected by the combination of symmetry and topology. If the symmetries are explicitly broken by a perturbation, then the zero modes may split. This is precisely the reason the Dirac theory and the precise honeycomb lattice model differ, and also the reason for the Zeeman splitting of the zero modes in the Dirac theory. This synergistic protection, while clearly more fragile than the topological protection of a single zero mode, may prove important in understanding many other physical systems beyond those we discuss here.

We have also generalized the known connection between topological zero modes bound to vortex cores and at sample edges in the well studied ordinary p_x+ip_y state. We have shown that in quite general settings, with the possibility of symmetry mandated degeneracy included, zero modes bound to vortices and edges should be *identified*.

Our analysis was limited to a number of presumed pairing states for fermions on the honeycomb lattice, but similar phenomena may be uncovered in other states involving the honeycomb lattice. In particular Refs. 39 and 40 have discussed noncondensate models on the honeycomb lattice with vortices possessing zero-mode bound states in their core. In both cases only a vortex calculation was carried out, and given our general observation that vortex-core bound zero modes should be identified with edge state zero modes, we expect these zero modes to appear at sample edges in the models of Refs. 39 and 40. In Ref. 40 the authors found that there is a *single* zero mode bound to the vortex core. Another related model which exhibits topological zero modes at sample edges is the Kane-Mele model,[41] which both in the precise lattice model, as well as in a continuum limit,[42] exhibits edge state zero modes (in the continuum case, for an armchair boundary—the zigzag boundary suffers from the same problems we pointed out in Sec. VI). Finally, we mention a very recent publication[43] finding zero modes bound to vortices in a bilayer-graphene exciton condensate. As in our case, the zero modes turn out to split in the precise lattice

model. We suspect that other interesting possible states of matter on the honeycomb lattice geometry exist, as well as in three-dimensional geometries that supply the common ingredient in all these models—the Dirac nodes in the lattice band structure. The physics of a three-dimensional version of the Kane-Mele model[44] is realized in $Bi_{1-x}Sb_x$, as recently probed in Ref. 45, and following this work Ref. 46 has suggested that Majorana fermion zero modes should appear at the interface between a topological insulator and an *s*-wave superconductor.

ACKNOWLEDGMENTS

We would like to acknowledge C. Chamon, D. Novikov, N. Read, and R. Sensarma for illuminating discussions. This work was supported by the NSF through Grant No. DMR-0803200 and through the Yale Center for Quantum Information Physics.

APPENDIX: SPINLESS $p+ip$ CONDENSATE

In this appendix we analyze the spinless p_x+ip_y phase mentioned briefly in the main text. We will find that this phase in some geometries will posses zero modes, but these are *bulk states* rather than bound states.

1. SNS junction

In this subsection we will analyze the SNS junctions in the spinless p_x+ip_y phase. We consider here only wave functions that are uniform in the direction parallel to the SNS junction boundaries, and find in stark contrast to the spin-singlet phases that no zero modes exist. The steps of our analysis follow closely those of the SNS calculations for the spin-singlet phases, and so we will describe our calculations in minimal detail.

With a (piecewise) uniform pairing function, combining the kinetic energy [Eq. (21)] and the spinless p_x+ip_y pairing terms [Eq. (24)] yields a BdG equation of the form

$$\mathcal{H}_{\mathrm{BdG}}\psi = E\psi = \{\mu\omega^z - iv\hat{D} + \tau^x\Delta\eta^z\hat{D}[\omega^x\cos(\phi) + \omega^y\sin(\phi)]\eta^y\}\psi, \tag{A1}$$

where we have dropped the two subscript from both the order-parameter phase and magnitude, to avoid clutter.

We consider only states that are uniform in the direction parallel to the SNS junction boundaries, and use the same unitary transformation $U(\alpha)$ to rotate the angle between the SNS boundaries and the y axis $\alpha\to 0$, in the operator $\hat{D}(\alpha)$ appearing in both the kinetic energy and the pairing terms. All other parts of the BdG Hamiltonian remain invariant, and as long as we ignore quadratic correction (25), we can simply set $\alpha=0$. The BdG equations reduce to

$$\{\mu\omega^z - E - iv\eta^x\partial_x + \tau^x\Delta i\partial_x[\omega^x\cos(\phi) + \omega^y\sin(\phi)]\}\psi = 0. \tag{A2}$$

As before, we will work in the London gauge which we can get by applying the unitary transformation $\mathcal{O}=e^{-i(\phi/2)\omega^z}$. We are left with

$$[\mu\omega^z - E - iv\eta^x\partial_x + \tau^x\Delta i\partial_x\omega^x]\psi = 0, \tag{A3}$$

from which it is clear that we can choose solutions that are eigenstates of both η^x and τ^x, such that $\eta^x\psi=\eta\psi$ and $\tau^x\psi=\tau\psi$. The BdG equations then can be reorganized in the form $i\partial_x\psi=A\psi$ with

$$A = \frac{1}{v^2-\Delta^2}\begin{pmatrix} v\eta(E-\mu) & \Delta(E+\mu)\tau \\ \Delta(E-\mu)\tau & v\eta(E+\mu)\end{pmatrix}. \tag{A4}$$

The eigenvalues of the matrix A are $vE\eta\pm\sqrt{\Delta^2E^2+\mu^2(v^2-\Delta^2)}$, and since we expect $v\gg\Delta$, the eigenvalues will in general be *real* numbers. As a consequence, we can only have solutions of ψ that are exponentials of purely imaginary arguments. As a result, no bound states can appear—these require some exponential decay of the wave function.

2. Edge geometry

We will now address the edge geometry in the spinless p_x+ip_y phase. Starting form the BdG Eq. (A1), with the phase chosen as $\phi=0$, and assuming a transverse momentum q, such that $\psi=e^{iqy}\psi(x)$. The reduced BdG equations are

$$[\mu\omega^z - iv\hat{D} + \tau^x\Delta\eta^z\hat{D}\omega^x\eta^y - E]\psi = 0, \tag{A5}$$

with $\hat{D}=\eta^x\partial_x+\omega^z\eta^y\partial_y$. Reorganizing the BdG equations yields

$$[\mu\omega^z - E + vq\eta^y\omega^z - q\Delta\tau^x\eta^z\omega^y]\psi = i[v\eta^x - \Delta\tau^x\omega^x]\partial_x\psi. \tag{A6}$$

Using the identity $[v\eta^x-\Delta\tau^x\omega^x]^{-1}=\frac{1}{v^2-\Delta^2}[v\eta^x+\Delta\tau^x\omega^x]$, we bring the equation to the form $\partial_x\psi=A\psi$, with

$$A = -i\left[\frac{1}{v^2-\Delta^2}(v\eta^x + \Delta\tau^x\omega^x)(\mu\omega^z - E) + iq\omega^z\eta^z\right]. \tag{A7}$$

We are free at this stage to choose solutions that are eigenstates of $\tau^x\psi=\tau\psi$, so we simply replace $\tau^x\to\tau$. Furthermore, it is useful at this point to denote $z=\frac{x\mu}{\sqrt{v^2-\Delta^2}}$, $\epsilon=\frac{E}{\mu}$, and $k=\frac{q\sqrt{v^2-\Delta^2}}{\mu}$, all of which are dimensionless quantities. We can also assume without loss of generality that $\mu>0, v>\Delta$, and $E\geq 0$. The BdG equations now become $\partial_z\psi=\tilde{A}$ with

$$\tilde{A} = -i\left[\frac{1}{\sqrt{v^2-\Delta^2}}(v\eta^x + \Delta\tau^x\omega^x)(\omega^z - \epsilon) + ik\omega^z\eta^z\right]. \tag{A8}$$

The four eigenvalues of the matrix $i\tilde{A}$ in this notation are

$$\pm\lambda_\eta = \pm\left[(1-k^2) + \epsilon^2\frac{v^2+\Delta^2}{v^2-\Delta^2} + \eta 2v\epsilon\frac{\sqrt{(v^2-\Delta^2)+\Delta^2\epsilon^2}}{v^2-\Delta^2}\right]^{1/2}, \tag{A9}$$

where $\eta=\pm 1$.

We are interested in exploring zero modes, so at this point we set $\epsilon=0$, to identify which eigenvalues can give solutions

that are exponentially decaying in the $z>0$ region. The eigenvalues of $\tilde{A}$ become $\pm\lambda_\eta = \mp i\sqrt{1-k^2}$. For exponentially decaying zero modes, we must therefore have $|k|>1$. In this regime, $q > \frac{\mu}{\sqrt{v^2-\Delta^2}}$. It is noteworthy that the nodes in the bulk spectrum for this phase occur in the continuum theory at precisely $\mathbf{q}=(\sqrt{3},1)\frac{\mu}{\sqrt{v^2-\Delta^2}}$. Therefore, these bound states may be identified with the bulk zero modes.

3. Vortex geometry

In this subsection we turn to explore whether zero modes exist bound to vortex cores in the spinless p_x+ip_y phase.

We start with the BdG equation $[\mathcal{H}_0+\mathcal{H}_3]\psi=E\psi$ with $\mathcal{H}_{0,3}$ from Eqs. (21) and (24). We choose the eigenstates to satisfy $\tau^x\psi=\tau\psi$, as in the SNS and edge geometries. We will model the vortex by assuming the form $i\Delta_2=\Delta(r)e^{+i\phi}$, with $\Delta(r)$ real (as for the spin-singlet p_x+ip_y case, the convention is different from earlier sections so that we can use the same ansatz for the polar angle dependence as for the s-wave case). Also, since it will prove convenient, we will assume that the order-parameter radial profile is piecewise uniform.

As in previous subsections, we find the ϕ dependence can be eliminated from the zero-mode problem by choosing the wave-function form

$$\psi(r,\phi) = e^{i\ell\phi}[u_1(r), e^{i\phi}u_2(r), v_1(r), e^{-i\phi}v_2(r)]^T. \quad \text{(A10)}$$

The reduced ODEs then involve only the radial coordinate, and can be cast in the form $\partial_r\psi=A\psi$, where

$$A = \frac{1}{r}\left(\ell\omega^z\eta^z - \frac{1}{2}\right) + \frac{1}{v^2-\Delta^2}\left[\frac{v^2}{2r}\eta^z + iv\eta^x(E-\mu\omega^z) - \frac{v\Delta\tau}{2r}i\omega^x\eta^y + \Delta\tau(Ei\omega^x - \mu\omega^y)\right]. \quad \text{(A11)}$$

For the purpose of showing that no bound-state zero modes exist, it will suffice to consider the asymptotic limit $(r\to\infty)$ alone. We neglect all terms in A that have a factor $1/r$

$$A = \frac{1}{v^2-\Delta^2}[iv\eta^x(E-\mu\omega^z) + \Delta\tau(Ei\omega^x - \mu\omega^y)]. \quad \text{(A12)}$$

Setting $E=0$, we find A has the eigenvalues $\pm i\frac{\mu}{\sqrt{v^2-\Delta^2}}$, which are purely imaginary. Therefore no bound states with zero energy are allowed. Thus, we conclude that no zero modes exist at the vortex core in this phase.

This particular calculation shows us that having a Dirac equation structure in the BdG equations is *not* a sufficient condition for topological zero modes to be present.

4. Numerics

In the previous sections of this appendix, we found that the edge state geometry can support some zero modes with a wave function concentrated at the at the edge. In contrast, in the vortex calculation found no bound-states zero modes. As we argued in this paper, in a fully gapped system, we expect a general correspondence between the edge-state spectrum and the vortex-core bound-state spectrum. This expectation does not hold here, presumably due to the fact that this phase is *not* fully gapped.

To verify that the vortex calculation result is correct (it uses the approximate continuum description) we employed the numerical methods of Sec. VIII. Using the precise lattice pairing function for the spinless p_x+ip_y phase, with a square lattice patch of 1824 lattice sites, we calculated the low-energy spectrum for the vortex state, with two different vortex-core sizes $R=0,\sqrt{5}$. We set the parameters $|\Delta|=0.5$ and $\mu=0.4$. The lowest energies divided by the de Gennes scale are $\frac{E}{\frac{\Delta^2}{E_F}} = \pm 0.027\,093\,9, \pm 0.055\,819\,3, \pm 0.076\,5734\ldots$, for $R=0$ and $\frac{E}{\frac{\Delta^2}{E_F}} = \pm 0.023\,496\,6, \pm 0.035\,054\,5, \pm 0.063\,066\,1\ldots$ for $R=\sqrt{5}$. The results in both cases are similar—we find low-energy states exist, far below the de Gennes energy scale, but *all* the states with energy below the de Gennes scale are delocalized bulk states and *not* concentrated near the vortex core. This result would indicate that the vortex calculation and edge-state calculations are not at odds—the zero modes found in the edge-state calculation are related to the bulk low-energy states that appear due to the nodes in the pairing function.

[1] N. Read and D. Green, Phys. Rev. B **61**, 10267 (2000).
[2] D. A. Ivanov, Phys. Rev. Lett. **86**, 268 (2001).
[3] V. Gurarie and L. Radzihovsky, Phys. Rev. B **75**, 212509 (2007).
[4] S. Tewari, S. Das Sarma, and D.-H. Lee, Phys. Rev. Lett. **99**, 037001 (2007).
[5] S. Tewari, S. Das Sarma, C. Nayak, C. Zhang, and P. Zoller, Phys. Rev. Lett. **98**, 010506 (2007).
[6] N. Read, Phys. Rev. B **79**, 045308 (2009).
[7] C. Nayak, S. H. Simon, A. Stern, M. Freedman, and S. Das Sarma, Rev. Mod. Phys. **80**, 1083 (2008).
[8] A. Stern, Ann. Phys. (N.Y.) **323**, 204 (2008).
[9] M. Dolev, M. Heiblum, V. Umansky, A. Stern, and D. Mahalu, Nature (London) **452**, 829 (2008).
[10] I. P. Radu, J. B. Miller, C. M. Marcus, M. A. Kastner, L. N. Pfeiffer, and K. W. West, Science **320**, 899 (2008).
[11] N. B. Kopnin and M. M. Salomaa, Phys. Rev. B **44**, 9667 (1991).
[12] G. E. Volovik, JETP Lett. **57**, 244 (1993).
[13] G. E. Volovik, JETP Lett. **70**, 609 (1999).
[14] G. E. Volovik, *The Universe in a Helium Droplet* (Clarendon, Oxford, 2003).
[15] M. Stone and R. Roy, Phys. Rev. B **69**, 184511 (2004).
[16] P. Fendley, M. P. A. Fisher, and C. Nayak, Phys. Rev. B **75**,

045317 (2007).
[17] A. Geim and K. Novoselov, Nature Mater. **6**, 183 (2007).
[18] L. F. Cugliandolo, E. Fradkin, and F. A. Schaposnik, Phys. Lett. B **224**, 407 (1989).
[19] P. Ghaemi and F. Wilczek, arXiv:0709.2626 (unpublished).
[20] C. Caroli, P. G. de Gennes, and J. Matricon, Phys. Lett. **9**, 307 (1964).
[21] B. Uchoa and A. H. Castro Neto, Phys. Rev. Lett. **98**, 146801 (2007).
[22] J. González, F. Guinea, and M. A. H. Vozmediano, Phys. Rev. B **63**, 134421 (2001).
[23] E. Zhao and A. Paramekanti, Phys. Rev. Lett. **97**, 230404 (2006).
[24] A. Vishwanath, Condens. Matter Phys. **5**, 37 (2001).
[25] J. Bardeen, L. N. Cooper, and J. R. Schrieffer, Phys. Rev. **108**, 1175 (1957).
[26] A. Altland and M. R. Zirnbauer, Phys. Rev. B **55**, 1142 (1997).
[27] M. F. Atiyah and I. M. Singer, Bull. Am. Math. Soc. **69**, 422 (1963).
[28] J. Alicea and M. P. A. Fisher, Phys. Rev. B **74**, 075422 (2006).
[29] A. H. Castro Neto, F. Guinea, N. M. R. Peres, K. S. Novoselov, and A. K. Geim, Rev. Mod. Phys. **81**, 109 (2009).
[30] L. Brey and H. A. Fertig, Phys. Rev. B **73**, 235411 (2006).
[31] A. R. Akhmerov and C. W. J. Beenakker, Phys. Rev. B **77**, 085423 (2008).
[32] A. Shailos, W. Nativel, A. Kasumov, C. Collet, M. Ferrier, S. Gueron, R. Deblock, and H. Bouchiat, EPL **79**, 57008 (2007).
[33] H. B. Heersche, P. Jarillo-Herrero, J. B. Oostinga, L. M. K. Vandersypen, and A. F. Morpurgo, Nature (London) **446**, 56 (2007).
[34] N. B. Hannay, T. H. Geballe, B. T. Matthias, K. Andres, P. Schmidt, and D. MacNair, Phys. Rev. Lett. **14**, 225 (1965).
[35] H. Kempa, Y. Kopelevich, F. Mrowka, A. Setzer, J. H. S. Torres, R. Hohne, and P. Esquinazi, Solid State Commun. **115**, 539 (2000).
[36] Y. Kopelevich, P. Esquinazi, J. H. S. Torres, and S. Moehlecke, J. Low Temp. Phys. **119**, 691 (2000).
[37] E. Grosfeld, N. R. Cooper, A. Stern, and R. Ilan, Phys. Rev. B **76**, 104516 (2007).
[38] C. J. Bolech and E. Demler, Phys. Rev. Lett. **98**, 237002 (2007).
[39] I. F. Herbut, Phys. Rev. Lett. **99**, 206404 (2007).
[40] C.-Y. Hou, C. Chamon, and C. Mudry, Phys. Rev. Lett. **98**, 186809 (2007).
[41] C. L. Kane and E. J. Mele, Phys. Rev. Lett. **95**, 226801 (2005).
[42] K. Sengupta, R. Roy, and M. Maiti, Phys. Rev. B **74**, 094505 (2006).
[43] B. Seradjeh, H. Weber, and M. Franz, Phys. Rev. Lett. **101**, 246404 (2008).
[44] L. Fu, C. L. Kane, and E. J. Mele, Phys. Rev. Lett. **98**, 106803 (2007).
[45] D. Hsieh, D. Qian, L. Wray, Y. Xia, Y. S. Hor, R. J. Cava, and M. Z. Hasan, Nature (London) **452**, 970 (2008).
[46] L. Fu and C. L. Kane, Phys. Rev. Lett. **100**, 096407 (2008).